2009

Impact of intrafraction motion on post-mastectomy TomoTherapy of the chest wall

Shima Ito
Louisiana State University and Agricultural and Mechanical College, sito1@tigers.lsu.edu

IMPACT OF INTRAFRACTION MOTION ON POST-MASTECTOMY TOMOTHERAPY OF THE CHEST WALL

A Thesis

Submitted to the Graduate Faculty of the
Louisiana State University and
Agricultural and Mechanical College
in partial fulfillment of the
requirements for the degree of
Master of Science

in

The Department of Physics and Astronomy

by
Shima Ito
B.S., Bates College, 2005
May 2009

Acknowledgements

I owe everything I do to my parents, Drs. Akira and Hiroko Ito, as they gave me life to live and education to contribute. My father is my strength and my mother is my dedication. I thank Dr. Hogstrom for giving me many opportunities to become a Medical Physicist. I cannot thank him enough for the care and support that he has provided me and my family for the last few years. I could not have made it without Dr. Parker, a dedicated advisor who was as supportive as I could have ever asked for. I had a joy of working with Dr.Cheek to start up the project. I thank my committee members, Dr. Gibbons, Dr. Gonzalez, and Dr. Levine for their clinical inputs, technical support and contribution to my study. I thank my classmates Andrew, Chris, David, Jason, and Ricky. Their intelligence challenged me to think, their competiveness made me tougher, and their kind heart kept me sane. I thank Dr. Matthews, Dr. Sajo, and Dr. Wang for their guidance and humor. I thank April, Davelyn, Sarah, and Yvonne for their administrative support and patience. I thank Mary Bird Perkins Cancer Center for letting me use their facility and equipments. I thank dosimetry team at MBPCC, especially Eddie, Chad, and Frank for their professional input and help with treatment planning. I thank radiation therapy team at MBPCC, especially Amy, James, Michael, and Yolanda for helping me with TLD patient measurements. I thank Physics team at MBPCC especially Connel for his extensive knowledge and patience to listen. I thank LSU for supporting me 4 years as a graduate student.

Table of Contents

List of Tables

List of Figures

Abstract

Purpose: The present work investigates the impact of intrafraction motion of the chest wall due to respiration on Post Mastectomy Radiotherapy (PMRT) with TomoTherapy. The hypothesis of this work is that the impact of intrafraction motion on TomoTherapy PMRT will be insignificant as (1) the largest intrafraction movement of the chest wall (CW) in the medial-lateral, anterior-posterior, and superior-inferior dimensions will not exceed 1 cm and (2) that 95% of in-vivo CW point doses on the patient surface will be within 5% of calculated dose and all doses within 10% of calculated dose.

Methods: 4DCT scans were acquired and intrafraction motion of the CW near mastectomy scar was analyzed for 5 PMRT TomoTherapy patients. In-vivo patient CW dose measurements, acquired for clinical purpose using TLD were analyzed. Measured dose was compared to the TomoTherapy calculated dose. Daily MVCT images were collected and the correlation between the amount of air cavity between CW skin and the bolus and the dose difference between TLD measured and calculated dose was studied for each patient. Surface dose measurement using a CW anthropomorphic phantom was performed to add confidence to the patients' data.

Results: The maximum anterior posterior (ant-pos) CW movement of our five patients did not exceed 0.15 cm. 28% of the TLD measured doses differed from the calculated dose by more than 5%, and 2% of all data differed from the calculated dose by more than 10%. Slight positive correlation between air cavity between bolus and the CW surface and measured dose difference was observed for both patients' and phantom data.

Conclusions: The result of this work indicates that the impact of intrafraction motion on TomoTherapy PMRT will be insignificant. Discrepancies between TLD measured CW point dose and calculated dose, but overall, the average dose differences were within 5%. Air cavities created between the bolus and the CW may impact on cause underdosing of the CW surface.

Chapter 1
Introduction

I. Background and Significance

A. Post-Mastectomy Radiation Therapy

1. Overview

Breast cancer is the most commonly diagnosed non-dermatologic cancer and the second leading cause of cancer-related death among women in the United States. The American Cancer Society estimated that 182,460 new cases of invasive breast cancer would be diagnosed among women, and approximately 40,480 women were expected to die from breast cancer in 2008. (American Cancer Society Inc. 2007-2008) Primary therapy for breast cancer generally involves lumpectomy and radiotherapy or modified radical mastectomy. Post mastectomy radiotherapy (PMRT) refers to comprehensive treatment of the chest wall and appropriate draining regional nodes. The rationale for PMRT is to improve overall survival and prevent recurrence of cancer in the chest wall, skin, mastectomy scar, and the regional nodes such as the axillary, supraclavicular and internal mammary nodes. Mastectomy followed by radiation therapy alone could result in long-term control of disease, even in patients with locally advanced breast cancer. (Strom *et al* 1991) Recent studies show a significant improvement in survival after PMRT in patients who received systemic therapy. (Overgaard *et al* 1997, Overgaard *et al* 1999) On the basis of these studies, a National Institutes of Health consensus panel recommended locoregional PMRT in patients with ≥ 4 positive axillary lymph nodes and/or T3 and T4 staged lesions. (Eifel *et al* 2000) A dose of 50 Gy in 25 fractions is usually prescribed.

2. Conventional PMRT Techniques

The complexity of PMRT in treating chest wall and regional nodes often poses many challenges to the radiation oncologist as the range of body habitus and close proximity of the internal mammary nodes (IMNs) to the heart often necessitate individualized treatment planning

with complex field arrangements. No single technique is accepted as a gold standard. Pierce et al. (2002) performed plan comparisons for 20 left-sided PMRT chest wall patients. Seven commonly used conventional techniques were planned for each patient, using a prescription of 50 Gy in 25 fractions to the chest wall (CW) and IMN targets. Radiationtherapy (RT) techniques (c.f. Figure 1.1) planned were: (1) standard tangents; (2) electron fields; (3) cobalt fields; (4) reverse hockey stick (RHS); (5) 30%/70% Photon/Electron mix; (6) 20%/80% Photon/Electron mix; and (7) partially wide tangent fields (PWTF). Diagrammatic presentations of seven RT techniques are shown in Figure 1.1. Dosimetric comparisons for the seven techniques were made using normal tissue complication probability prediction for pneumonitis and ischemic heart disease and dose-volume histogram analyses for normal and target issues. The study concluded that no one technique studied combined the best CW and IMN coverage with minimal lung and heart complication probabilities. Of the seven techniques studied, however, the use of PWTF's was found to produce the most appropriate compromise of PTV coverage and normal tissue sparing. In conclusion, the study recommended that the final selection of an RT technique should be based on the estimated risk reduction in locoregional recurrence and its potential impact on survival, the predicted complication risk for the patient, and the technique expertise available to implement complex treatment plans. (Pierce *et al* 2002) The study took neither IMRT nor TomoTherapy into consideration.

B. TomoTherapy

1. Overview

The TomoTherapy Hi-ART System® (TomoTherapy Inc., Madison, WI) is a radiotherapy machine designed to deliver intensity modulated radiotherapy (IMRT) using helical tomotherapy to perform image guidance using a fully integrated on-board megavoltage-CT (MVCT).

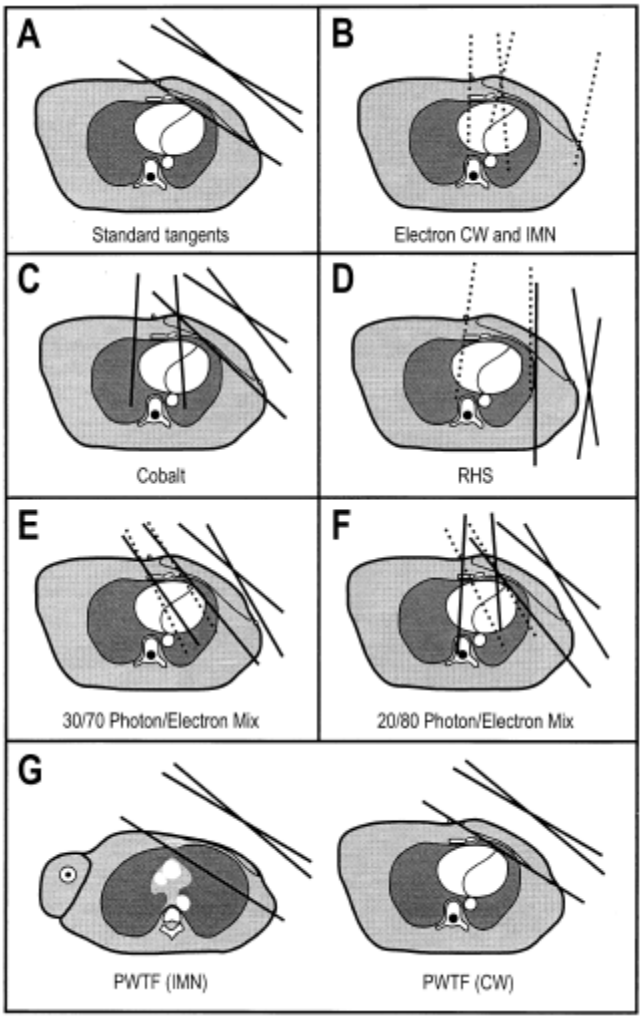

Figure 1.1. Diagrammatic presentation of RT techniques (Pierce *et al* 2002)

(Mackie *et al* 1993) The basic configuration of the TomoTherapy unit is illustrated in Figure 1.2. The source of radiation is an unflattened 6 MV x-ray beam produced by an in-line linear accelerator (linac) mounted on a continuously rotating CT-style ring gantry with a bore diameter of 85 cm. The beam is collimated to a fan beam that is 40-cm wide by 1.0, 2.5, or 5.0 cm long, defined by a pair of x-ray jaws.

During treatment, the rotating fan beam radiation is delivered to the patient while the couch moves through the gantry in a longitudinal direction, resulting in a helical delivery pattern. (c.f. Figure 1.3) Intensity modulation is achieved by a 1-D multi-leaf collimator (MLC) with 64

binary leaves for which each leaf position is either open (i.e., letting the beam pass through) or closed (i.e., blocking the beam). The leaf width is 0.625 cm at isocenter.

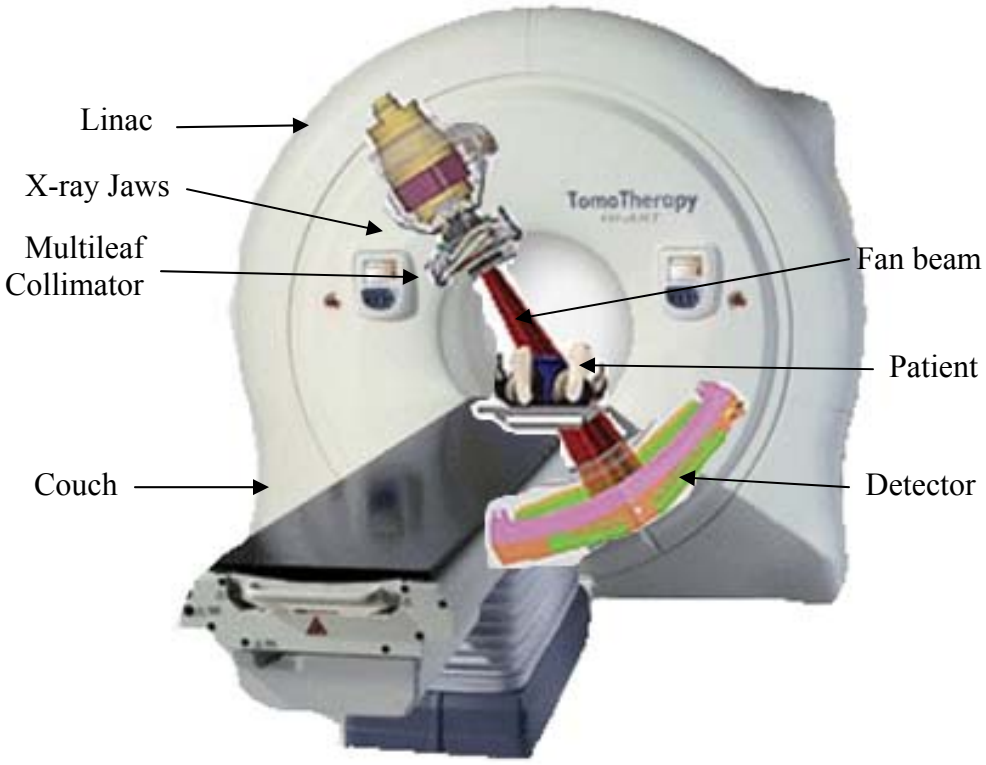

Figure 1.2. Picture of TomoTherapy unit. Linear accelerator is mounted to a gantry with a bore diameter of 85 cm. The axis of rotation is also 85 cm from the x-ray target source.

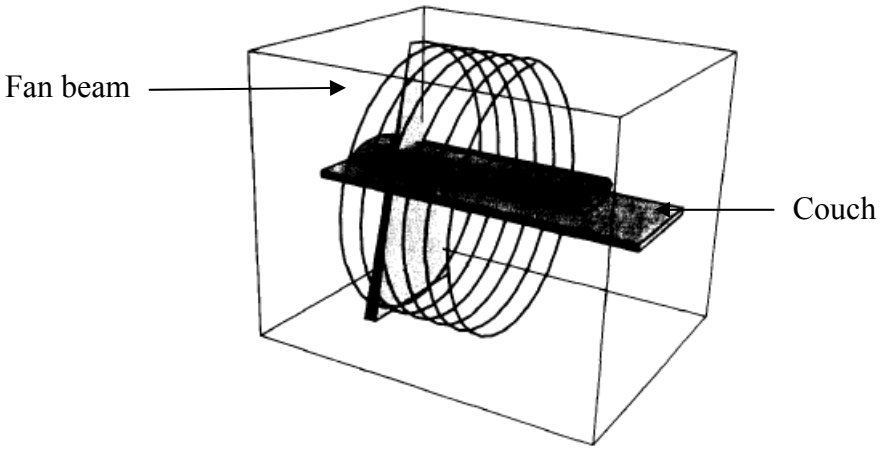

Figure 1.3. An illustration of helical delivery pattern. (Mackie *et al* 1993)

Non-uniform beam intensity is achieved by varying the leaf opening time. A beamlet is defined as that portion of the radiation beam defined by one projection angle and one open MLC leaf (e.g. 0.625 cm x 2.5 cm). During beamlet optimization, beam weight is optimized for 51 gantry mini arcs (7.06°) or projections per gantry rotation, making a total of 3,264 possible beamlets in each rotation. The large number of incident beam angles (51) and beamlets (3,264) allows delivery of highly conformal dose distributions. The total number of possible beamlets is 3,264 x number of gantry rotations, n, given by

$$n = \frac{field\ length}{jaw\ width \times pitch}$$

when pitch is defined as the ratio of the couch travel distance per rotation to the field size defined at the axis. Kissick et al. (2005) studied the helical tomotherapy thread effect and determined that a pitch of 0.86/n, when n is on integer, will minimize the ripple. (Kissick *et al* 2005) A pitch of 0.287 (0.86/3) is typically used at MBPCC.

The other unique capability of the TomoTherapy Hi-Art is its real-time imaging system. A conventional xenon ion chamber CT detector system is located 180˚ from the treatment linac. The detector reads the amount of exit radiation as the beam passes through the patient and the couch. The collected megavoltage transmission data is used for generating MVCT images for the patient registration (Fitchard *et al* 1998a, Fitchard *et al* 1998b, Lu *et al* 1999) and potentially for dose reconstruction (McNutt et al 1996a, McNutt et al 1996b, Olivera et al 1998). In TomoTherapy MVCT, the linac energy is reduced to a nominal energy of 3.5 MV. Because of this fairly high energy when compared to a regular kilovoltage CT (kVCT) scan, the image acquired with TomoTherapy is referred to as a megavoltage CT (MVCT) scan.

2. TomoTherapy as a Superficial Treatment

Typically, IMRT has been used to treat deep-seated lesions such as lung, head and neck, and prostate cancer. However, recent studies have shown that TomoTherapy IMRT (helical tomotherapy) may be a viable alternative to treat superficial lesions that have been traditionally treated with electrons, static photon beams, or a combination of the two.

Orton et al. (2005) compared TomoTherapy and conventional linac-based technique plans for total scalp irradiation. Their results showed improved critical structure dose and more homogeneous target dose with TomoTherapy plans compared to the traditional linac-based electron-photon technique of Tung et al. (Tung *et al* 1993). Dosimetric and in-vivo dose verification studies were performed to evaluate the efficacy of utilizing TomoTherapy to treat anal adenocarcinoma patients who have undergone abdominoperineal resection. (Han *et al* 2008) In their study, TomoTherapy plans were compared to step-and-shoot IMRT technique plans. TomoTherapy plans showed significantly better target dose homogeneity and dose conformity around the PTV. Diode-based dose measurements on the surface of the scar located in the perineal area and the anterior surface of the external genitalia area all showed reasonable agreement (-3.4% to 5.5%) with the calculated dose.

Craniospinal irradiation has been traditionally treated using static parallel opposed photon beams for the brain and base of brain and using static posterior field(s) of electron (children) or photon (adult) beam for the spinal theca. (Maor *et al* 1985) However, the traditional technique has inherent dosimetric variations due to field abutment and requires multiple room entries and couch/gantry rotation. Tomblyn et al. (2007) compared dose plans of a linac-based conventional craniospinal irradiation technique to that delivered by TomoTherapy. The TomoTherapy technique resulted in superior PTV dosimetry, with a higher minimum dose and better dose conformity. Maximum doses to normal tissues were lower compared to the traditional linac-

based technique. Another comparison by Lee et al. (2007) showed that TomoTherapy was comparable to segmented multi leaf collimator (sMLC) delivery for the treatment of parotid gland tumors. The general conclusions of their paper is that TomoTherapy is an attractive alternative to conventional fixed beam techniques because (1) it minimizes field abutment issues and (2) it offers equal or superior dose distribution (uniform PTV dose and less dose to critical structures). On the down side, TomoTherapy indicates a greater volume of low dose that could have implications for secondary cancers.

For TomoTherapy to be used effectively to treat superficial lesions, it is essential that the treatment planning system (TPS) accurately calculate doses at or near the skin surface. Cheek et al. (2006) evaluated superficial dose calculations using a cylindrical film phantom. The phantom included removable transverse and sagittal film cassettes as shown in Figure 1.4a. TomoTherapy treatment plans were developed for three superficial PTVs (2, 4, and 6 cm deep radially by 90° azimuthally by 4 cm longitudinally). A treatment planning image of the 2 cm thick PTV is shown in figure 1.4b. The superficial plans were measured with Kodak (Eastman Kodak Co., Rochester, NY) EDR2 film and compared to the calculated dose distribution.

Results showed that the TomoTherapy TPS algorithm overpredicted the dose in the surface region (depths less than 1 cm) by as much as 9.5% of the prescribed dose. At depths greater than 1 cm, calculated and measured dose distributions agreed within 5% in the high-dose, low dose-gradient region and within 2 mm distance-to-agreement (DTA) in the high-dose gradient region. Figure 1.5 shows the depth dose comparisons for the 4 cm PTV. It is seen that the fluctuations are greater for the TomoTherapy calculated doses than the measured dose. These differences in the surface region may be due to (1) the discretization of the dynamic delivery and the heavily weighted surface pencil beams and (2) failure of the convolution/superposition

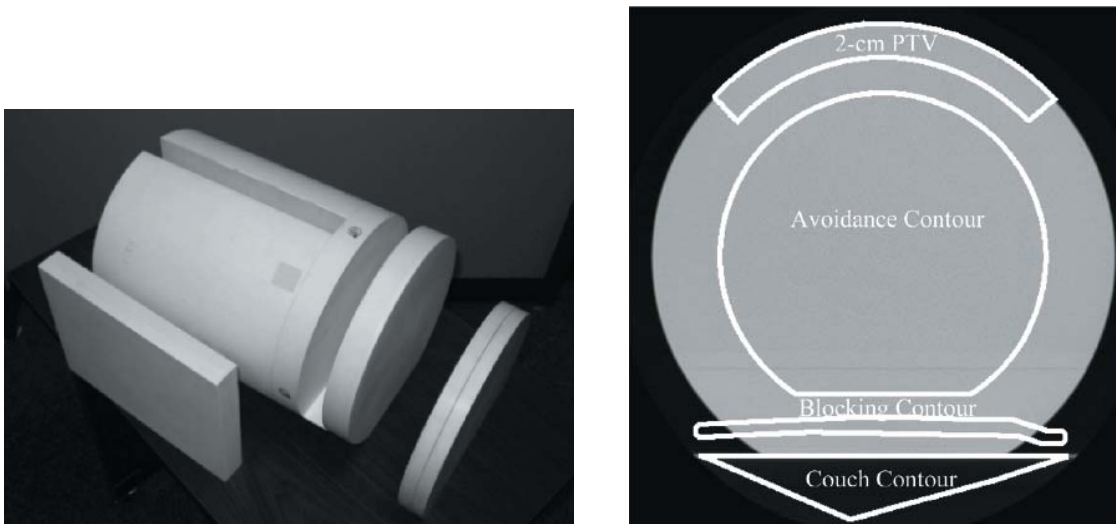

(a) (b)

Figure 1.4. Pictures of (a) 13.5-cm radius by 37.4-cm length white opaque high-impact polystyrene cylindrical phantom is depicted with axial and sagittal film cassettes removed from the phantom and (b) TomoTherapy treatment planning image showing the 2 cm thick PTV, avoidance, blocking, and couch contours. (Cheek *et al* 2006)

algorithm to account for reduced backscatter dose for highly oblique beam near the surface. Therefore, Cheek et al. (2006) recommended for clinical use that 1 cm of bolus be used on the patient surface to ensure that regions of dose inaccuracy greater than 5% underdose occur in the bolus, not in the target.

At MBPCC, PMRT TomoTherapy patients are treated with an approximately 1-cm thick Aquaplast RT® Bolus (Radiation Products Design, Inc., Albertville, MN), which produces a rigid shell around the patient. This not only ensures a greater accuracy in the calculated dose, but it also makes it possible to expand the PTV into the bolus to minimize the dosimetric effects of intrafraction (e.g., respiration) and interfraction motion (e.g., setup error), although expanding the PTV has a negative impact with normal tissue and lung receiving more dose unless bolus is used. Typical PTV expansion for CW TomoTherapy treatment is 1 cm anteriorly to include the bolus.

3. TomoTherapy as a PMRT Treatment

Ashenafi et al. (2006) compared TomoTherapy plans to conventional electron-photon mixed beam technique plans commonly used at Mary Bird Perkins Cancer Center for 5 PMRT patients. Plan comparisons were based on physician clinical judgment,

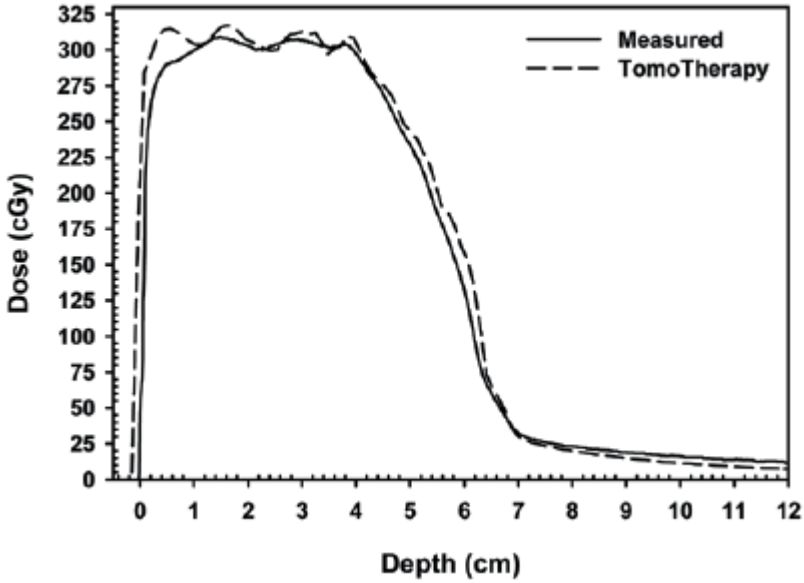

Figure 1.5. Comparison of TomoTherapy calculated with measured mid-arc depth dose curves for the 4 cm radially thick PTV. (Cheek *et al* 2006)

dosimetric values, and biological indices. In the study, the radiation oncologist rated four TomoTherapy plans superior to the conventional electron/photon beam treatment plan and one marginally superior and TomoTherapy was able to reduce high dose to the ipsilateral lung and heart, while delivering a more uniform dose distribution to the target volume. However, the TomoTherapy plans showed an increased risk for secondary cancer due to the contralateral breast, lung, and other normal tissue outside the target receiving an increased volume of low radiation dose. However, the treatment plans studied were planned on static patient CT data which do not take intrafraction and interfraction motions into consideration.

4. Previous TLD Dose Verification Study

After the initial TomoTherapy PMRT treatment, our radiation oncologist observed that the skin reaction of the PMRT patients treated with TomoTherapy appeared less severe than they were accustomed to seeing with conventional techniques. Based on this concern, the physician began requiring in-vivo TL dosimetry as a quality assurance procedure to compare measured and TPS calculated dose. On the first day of treatment, a radiation therapist marked a point on the CW near the mastectomy scar. TLD LiF powder (~45mg) in a cellophane wrapper, as shown in Figure 1.6(a), was taped onto the mark prior to MVCT registration, and the TLD position was photographed as shown in Figure 1.6(b). Upon completion of the fraction delivery, the TLD was removed. Calibration TLD's were exposed on the same treatment day on a 6MV linac for four different doses (100, 150, 200, and 250 cGy) that bracketed the daily fraction dose. The TLDs were read out, and the resulting thermoluminescence (TL) counts were converted to doses. In the Pinnacle[3] (v. 7.4f) TPS (Philips, Madison WI) TPS, a point of interest (POI) was added where the TLD was located by comparing the patient pictures and 3D skin rendering, as shown in Figure 1.6(c). The calculated POI dose was determined and compared to the TLD measured dose.

(a) (b) (c)

Figure 1.6. Pictures of (a) Sample TLD packet (LiF powder enclosed in a cellophane wrapper) used in measurements; (b) patient with TLD packet taped on the CW near the mastectomy scar; (c) 3D skin rendering with POI corresponding to the location of the TLD. The scar is contoured and the bolus is not shown.

The prescription dose, the calculated dose from the treatment planning system, the mean (±σ) measured TLD dose, and the percentage difference between the calculated and measured doses for each of 9 TomoTherapy PMRT patients are shown in Table 1.1. Plots of the calculated and the mean measured TLD doses versus fraction number for each of the 9 patients are shown in Figure 1.7 (a-i). The number of TLD measurements acquired throughout the course of treatment ranged from 5 to 25 per patient. Overall for the 9 patients, the TLD measured (delivered) dose was less than the calculated (TPS) dose by 4.0 % and the standard error of the mean was 4.7 %. This result raised a clinical concern since some patients were underdosed by more than 5 %. However, two patients (cf. Fig 1.7c and 1.7f) showed an underdose by 8.5 % and 12.2 %, respectively, with the other 7 patients showing the TLD measured (delivered) dose was less than the calculated (TPS) dose by 1.9 % and the standard error of the mean was 0.9 %.

Table 1.1. Prescribed, calculated, mean TLD measured doses for a point on patients CW, % difference was obtained by 100 x (measured dose – calculated)/calculated. The number of sample points (N), mean (D_{avg}), and standard deviation of the mean (σ) are given for each patient. (Fx: fraction)

	Prescribed Doses		Calculated Doses	Measured Doses		Difference
Patient	fxs[#]	fx Dose[cGy]	[cGy]	N	Davg ± σ [cGy]	[%]
1	30	220	230.2	14	224.4 ± 13.5	-2.5 ± 5.8
2	25	200	202.9	5	201.2 ± 8.0	-0.8 ± 4.0
3	25	200	201.4	15	184.3 ± 11.4	-8.5 ± 5.7
4	25	200	208.7	25	198.0 ± 8.1	-5.1 ± 3.9
5	25	200	208.5	22	199.5 ± 8.6	-4.3 ± 4.1
6	25	200	218.9	22	192.3 ± 8.8	-12.2 ± 8.7
7	25	200	205	23	206.1 ± 6.0	0.5 ± 2.9
8	30	150	152	10	152.0 ± 6.5	0.0 ± 4.3
9	25	150	151.8	21	150.3 ± 5.9	-1.0 ± 3.4
					Mean ± σ	-4.0 ± 4.7
		Excluding patient 3 & 6, Mean ± σ				-1.9 ± 0.9

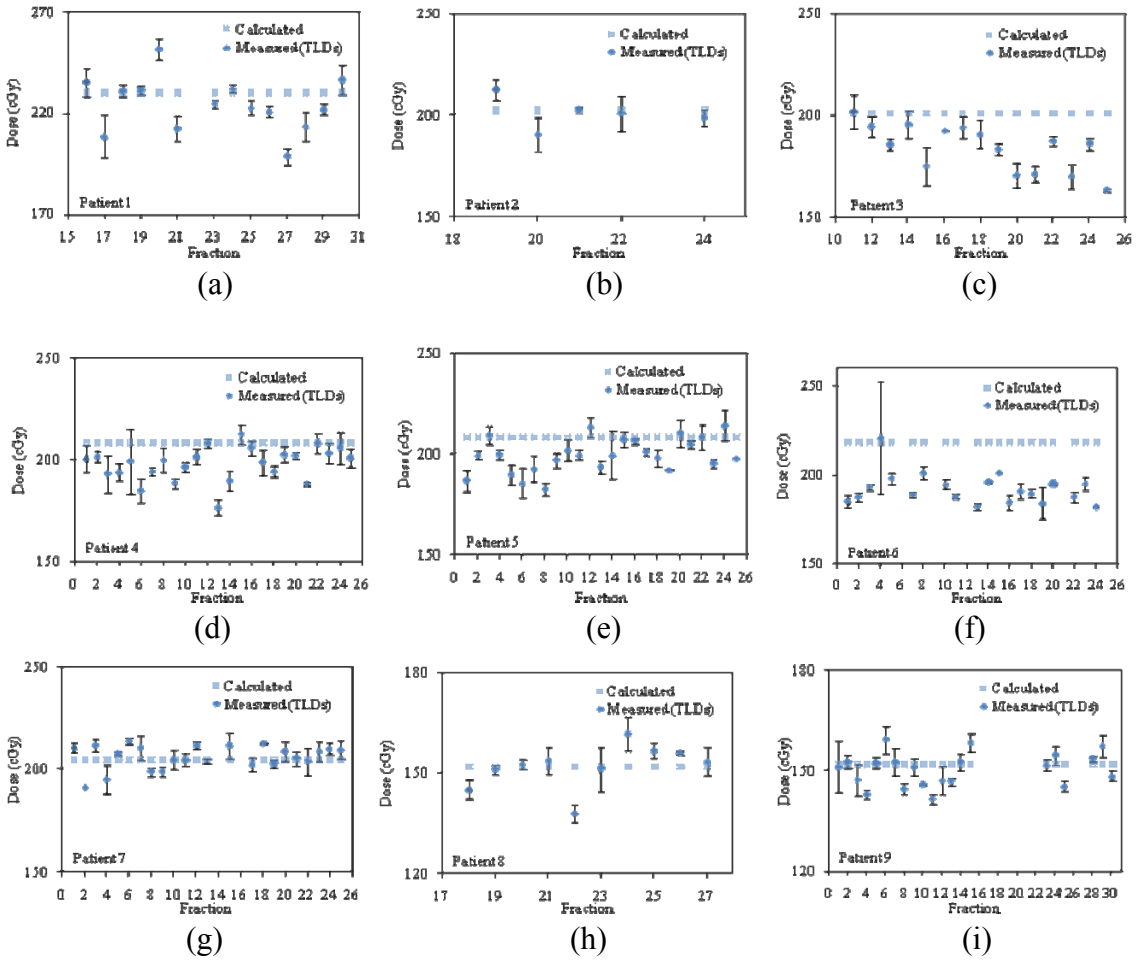

Figure 1.7. (a)-(i) Calculated doses (square) and mean measured TLD doses (diamonds) for 9 TomoTherapy PMRT patients.

Although 7 CW patients showed good agreement between measured and calculated doses (-1.9 ± 0.9 %), the cause of underdosing greater than 5 % were of clinical concern. This result compelled additional validation of the accuracy of TomoTherapy CW dose delivery by the clinical physics group, as well as an investigation of the possible sources of dose variation (e.g., intrafraction motion of CW, air cavities created between the skin surface and bolus).

5. Factors that Affect Dose Variation

a. Intrafraction Motion

Organs of the thoracic and abdominal regions are known to move with breathing. Previous works have observed and measured the movement of the organ and the tumor of different sites such as lung, diaphragm, pancreas, liver, and breast via ultrasound, CT, 4DCT,

MR, and fluoroscopy. (Keall *et al* 2006) However, none of the studies focused on chest wall movement in PMRT. Since our clinicians are in the early stages of using TomoTherapy for PMRT and understanding the range of CW movement was desirable, physicians ordered 4DCT scans to evaluate chest wall motion. Also TL dosimetry to measure delivered dose on the patient's skin surface was continued.

4DCT can be accomplished by oversampling CT data acquisition for each slice throughout the breathing cycle. During several CT tube rotations projection data are collected in axial cine mode for the duration of the patient's respiratory cycle in a fixed couch position. Our GE Light Speed RT (SN 55011) can scan 16 simultaneous axial images of 2.5 mm slice thickness, which means a 4 cm body section (16 x 2.5 mm) can be scanned at one time. Multiple images are then reconstructed per slice that are evenly distributed over the acquisition time. After data acquisition at one couch position is completed, x-rays are turned off and the couch advances to begin data acquisition again. This is repeated until full coverage of the scan length has been obtained (Rietzel *et al* 2005).

For external registration, the Real-Time Position Management (RPM) Respiratory Gating System (Varian Medical Systems, Palo Alto, CA) was used to monitor and record respiratory motion based on infrared reflecting markers on the patient's abdomen. The markers were illuminated by infrared emitting diodes, and images of the markers were captured by a camera at 30 frames per second. The RPM system (marker box and camera system) in the CT room is shown in Figure 1.8.

The GE Advantage 4D version 1.6 software is used to sort images into temporally coherent volumetric image data sets. The software reads the reconstructed images as well as the

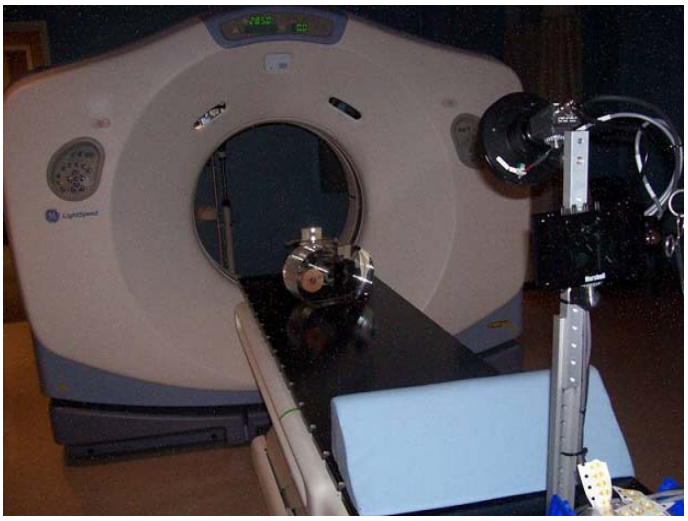

(a)

(b)

Figure 1.8. Pictures of (a) RPM respiratory gating system and (b) infrared emitting diodes surrounding a camera

corresponding RPM respiratory data file. In building a spatially coherent volumetric data set, a specific respiratory phase has to be chosen. At MBPCC, we divide one breath cycle into 10 equally spaced phase bins, with 0% being the inhalation peak and 50% the exhalation peak. For each couch position, the reconstructed image with the respiratory phase nearest the requested phase is selected by the GE software to form the 3D data set for a given time instant (Pan *et al* 2004). Figure 1.9 shows a qualitative illustration of scan and reconstruction. In the illustration, there are four images reconstructed per sample for a four-slice multi-slice (MSCT) and eight samples in a respiratory cycle. Once sorted into phases, a CT volume is exported into DICOM format for each of the selected phases.

There are considerable concerns regarding the use of IMRT with targets affected by intrafraction motions. One concern is that the increased conformality of IMRT dose distributions can potentially lead to underdoses at the border of the target volume due to intra/interfraction motion. However, Yu et al. (1998) showed that fluence variations within a moving target tend to average out over the typical course of 30 fractions, when one assumes that the breathing phrase

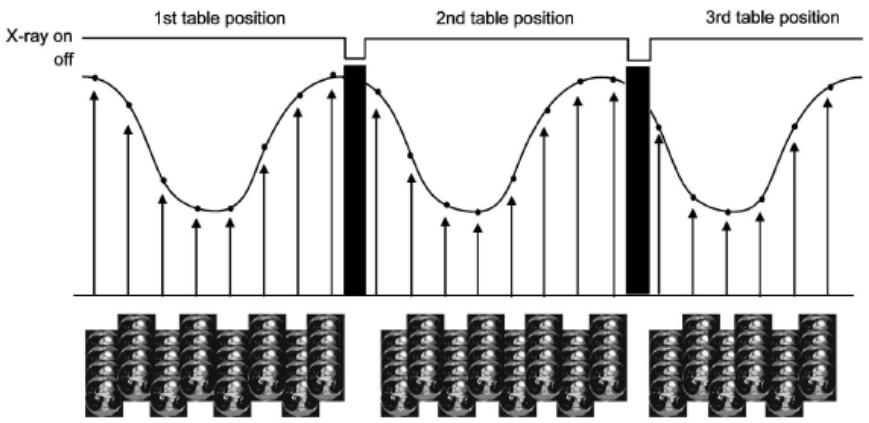

Figure 1.9. An illustration of scanning and image reconstruction. (Pan *et al* 2004)

or frequency is random from day to day. An investigation of TomoTherapy beam delivery suggested that the dose variations caused by intrafraction respiratory motions of typical breathing (amplitude is smaller than 1 cm peak to peak) is minor for the helical beam with a 2.5 cm slit and 4 rpm rotational speed (Yang *et al* 1996). Another motion phantom study on TomoTherapy by Kanagaki et al. (2007) focused on the dosimetric impact of respiratory motion in the superior/inferior dimension with varied treatment unit parameters. The study validated helical TomoTherapy as a safe technique for treating moving tumors given the current standard of margin expansion.

Interfraction motion is also a critical issue. A variety of image-guided radiation therapy (IGRT) systems have been developed that allow verification and correction of the target position prior to each treatment.

The utility of TomoTherapy MVCT scanning prior to the treatment fraction is particularly important when the patient's anatomy may vary between fractions, as the treatment can be significantly degraded if changes in the patient's anatomy are not detected (Ruchala *et al* 2004). It is advantageous to have this scanning technology incorporated into the therapy machine, so that the patient need not move between the CT scan and the treatment delivery. Because of this feature, interfraction movement can be minimized.

To confidently treat PMRT patients with TomoTherapy, it is important to show that intrafraction motions of chest wall have little impact on the dose distribution and that doses are delivered accurately. Intrafraction motion can be evaluated via 4DCT. Interfraction motion can be accounted for by acquiring an MVCT scan every day prior to the fraction delivery for PMRT patients. Based on MVCT, appropriate shifts can be made to align the patient's anatomy, then overlay kVCT based dose distribution for final adjustment. All the MVCT data are stored so that dose re-computation can be performed if needed.

b. Air Cavities

The bolus is used to provide adequate dose buildup over the skin surface. In TomoTherapy PMRT, approximately 1 cm thickness of solid thermoplastic bolus (Aquaplast RT® Custom Bolus, WFR/Aquaplast Corp.) is used. The bolus is molded to fit the patient's CW contour by a technician prior to the planning CT acquisition. Also, having the patient scanned with bolus allows the expansion of the PTV above the skin without having a negative impact on the optimization of beamlet fluence patterns near the skin. When constructing the bolus, it is important to leave minimal air cavities between the bolus and the patient CW. The air cavities between the absorber and the surface could result in electronic disequilibrium and decreased dose to the CW.

Based on clinical experience at MBPCC, throughout the typical PMRT CW treatment course of 5 weeks, the bolus tends to dry and shrink, which slightly change its shape, likely increasing air cavities between the bolus and patient skin surface. Figure 1.10 shows an example of increasing air cavity as the treatment progresses (fraction 11 vs. fraction 25) on patient 3, from previous TLD dose verification study, whose averaged measured dose was 8.5% lower than the calculated dose from our previous TLD study. Obese patients tend to exhibit more severe irregularities in skin surface, and the amount of air cavities created is significant enough to result

in dose deficit. This is not taken into account upon planning since there are no air cavities at a time of CT acquisition. The size of air cavities depends on each patient's surface anatomy, set-up parameters, and how much the bolus changes in shape. It is extremely difficult to combine all these effects and predict the dose distribution. However, with the existing daily MVCT data sets and in-vivo TLD measurement data, we may be able to investigate the dose around the superficial regions of air cavities.

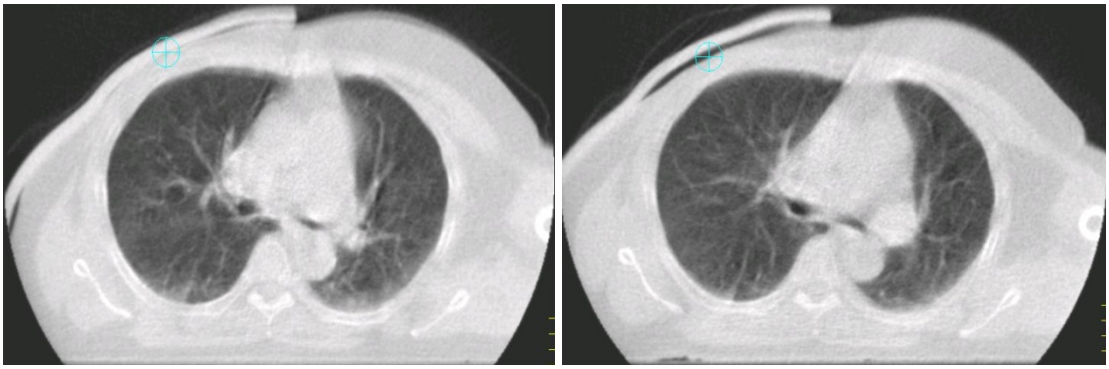

Figure 1.10. MVCT images of patient 3 taken prior to the treatment at (a) fraction 11 compared to (b) fraction 25 which increase of air cavity is observed. Light blue cross is where TLD package was taped.

The purpose of the present study is to study in-vivo TL dose measured data for patients treated using TomoTherapy for PMRT and to investigate possible sources of dose variation from planned dose distribution such as intrafraction motion and air cavities.

II. Hypothesis and Specific Aims

A. Hypothesis

Impact of intrafraction motion on TomoTherapy Post-Mastectomy Radiotherapy (PMRT) will be insignificant as (1) the largest intrafraction movement of the chest wall (CW) in the medial-lateral, anterior-posterior, and superior-inferior dimensions will not exceed 1 cm and (2) that 95% of in-vivo CW point doses on the patient surface will be within 5% of calculated dose and all TLD measured doses within 10% of calculated dose.

B. Specific Aims

Aim 1. Characterize intrafraction motion of patients

Clinically acquired 4DCT and 3DCT scan data for 5 CW patients will be analyzed and intrafraction motion will be determined.

Aim 2. Analyze clinical dose measurements at multiple points during treatment and compare with calculated dose:

Clinical TLD data for 5 CW patients, acquired for 15 fractions, will be compared with calculated dose.

Aim 3. Measure surface dose at multiple points on phantom and compare with calculated dose:

TLD measurement data for anthropomorphic CW phantom will be compared with calculated dose.

Chapter 2
Methods and Materials

I. Aim 1

The purpose of aim 1 was to characterize intrafraction CW motion of TomoTherapy patients. The 3DCT and 4DCT scan data for 5 CW TomoTherapy acquired for clinical purposes with a GE LightSpeed RT were analyzed in this study. The static 3DCT scan was used for treatment planning, and the 4DCT scan was used to evaluate chest wall motion due to breathing.

A. Clinical CT Simulation

1. Patient Marking

Prior to clinical scanning, a Vac-Loc (Civco Medical Solutions, Kalona, Iowa, USA) immobilization cushion was fabricated to ensure daily setup reproducibility on the TomoTherapy unit. Shown in Figure 2.1(a), the mastectomy scar was marked with a CT-SPOTS® line marker (Order code #118 Beekley Corp.) by a CT technologist. Once the scar was marked, 7-8 points surrounding the scar were marked with a permanent marker with uniform spacing approximately every 3-cm. A 2.3-mm diameter CT-SPOTS® pellet (Order code #120 Beekley Corp.) was placed on each of the points, as shown in Figure 2.1(b). These markers were used in the 4DCT images to assess chest wall motion throughout the breathing cycle.

2. Immobilization and Skin Bolus

At MBPCC, every PMRT TomoTherapy patient is treated with 1-cm thickness bolus, which serves two purposes. The first purpose is to provide charged particle equilibrium at the skin surface ensuring that the chest wall and scar receive the prescribed dose. The second purpose is to allow for the expansion of the PTV outside of this skin surface to account for chest wall motion and setup uncertainties. A solid thermoplastic bolus (Aquaplast RT® Custom Bolus, WFR/Aquaplast Corp.) was placed into hot water (~160 ºF) bath and allowed to soften. After the bolus was removed from hot water bath, the CT technologist molded the bolus to the

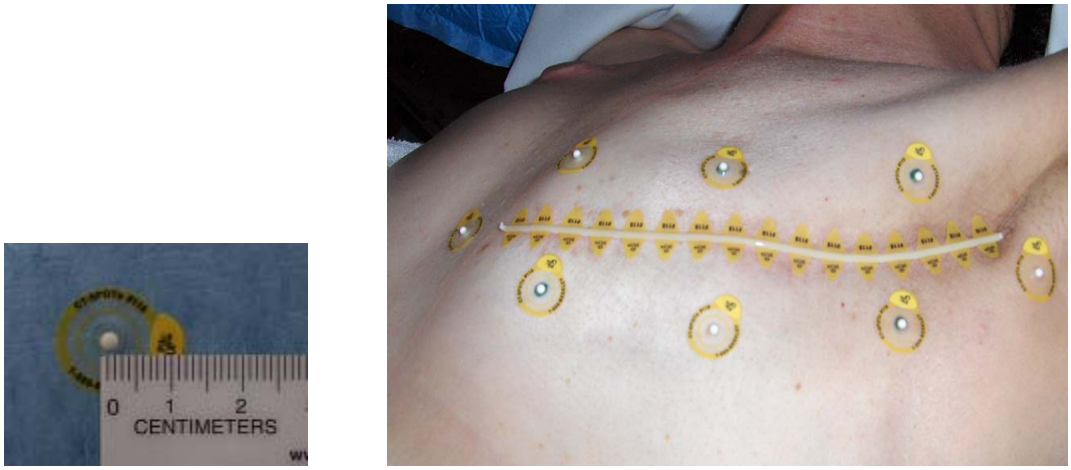

(a) (b)

Figure 2.1. Picture of (a) CT-SPOT® pellet and (b) patient CW with intrafraction movement points marked. CT-SPOT® line marker was placed to trace the mastectomy scar.

patient's CW ensuring it covered the entire expected PTV. Unnecessary bolus was cut off, laser alignment marks were drawn on the bolus, one near sternum and another one on lateral side. An example of the bolus with reference marks is shown in Figure 2.2.

B. CT Scan Acquisition

Once the pre-scan procedures were completed, the 3D scan was performed according to the institution's clinical scan protocol. The 3D scans for the patients, whose data is used in the present study, were taken at 120 kV and 80 mA.

The 4DCT dataset for the same patient was used strictly to evaluate the magnitude of chest wall motion throughout the breathing cycle to ensure that adequate PTV expansion was used. The 4DCT scan was acquired according to our in-house 4D scanning protocol.

To reduce unnecessary radiation dose to the patients, the scan range was limited to the volume including the CT-SPOTS pellets plus an approximately 2-cm margin inferiorly and superiorly to cover the projected maximum pellet travel when setting the cine scan range. Patients were given no specific instructions on their breathing pattern.

Figure 2.2. Picture of PMRT patient with bolus on right chest wall. Laser alignment marks in cross hair is drawn on the bolus, which indicates the patient will be aligned to match the marks with laser in the treatment room prior to their treatment. Vaclock immobilization device was fabricated to stabilize patient's right arm up in place.

C. Transferring CT Data

TomoTherapy PMRT planning was done on 3DCT images. By default, the TomoTherapy DICOM server down samples the CT images to 256 x 256 matrix. However, this is often too many data points for the optimizer to perform a beamlet optimization without error. MBPCC policy states that TomoTherapy patient plans will be planned using the finest dose grid and resolution available, but if that is not possible, the CT image resolution should be down sampled (reducing the matrix size, thus resulting in volume averaging of the CT data and reducing spatial resolution) prior to planning. Since our clinical standard for planning PMRT is to down sample the CT image resolution to 128 x 128 matrix in order to avoid any optimization error, the phantom image was down sampled accordingly. Hence, down-sampled CT scan data was imported into the TomoTherapy treatment planning system from the CT workstation (GE Discovery DT,) after the 3DCT scan was acquired. Regarding 4DCT data, the RPM files and 4DCT images were transferred to the Advantage Workstation® (AW) where images were sorted

into 10 different respiratory phases. CT data for each of the selected phases were exported in Dicom format and then imported on Pinnacle Treatment Planning System (TPS).

D. TomoTherapy PMRT Treatment Planning

PTVs, which included chest wall (CW), and regional lymph nodes such as the supraclavicular (SC), the internal mammary chain (IMN), and the axillary (AX) nodes, were contoured by our radiation oncologist (Renee Levine, MD) on the Pinnacle TPS for all five patients. For these patients, the PTV included the bolus to account for intrafraction breathing motion during treatment and for interfraction setup errors. Additionally the PTV extended approximately 5-mm into the lung, again to allow for intrafraction motion. A typical axial contour including the PTV is shown in Figure 2.3. ROIs were transferred from the Pinnacle workstation to the TomoTherapy TPS for treatment planning.

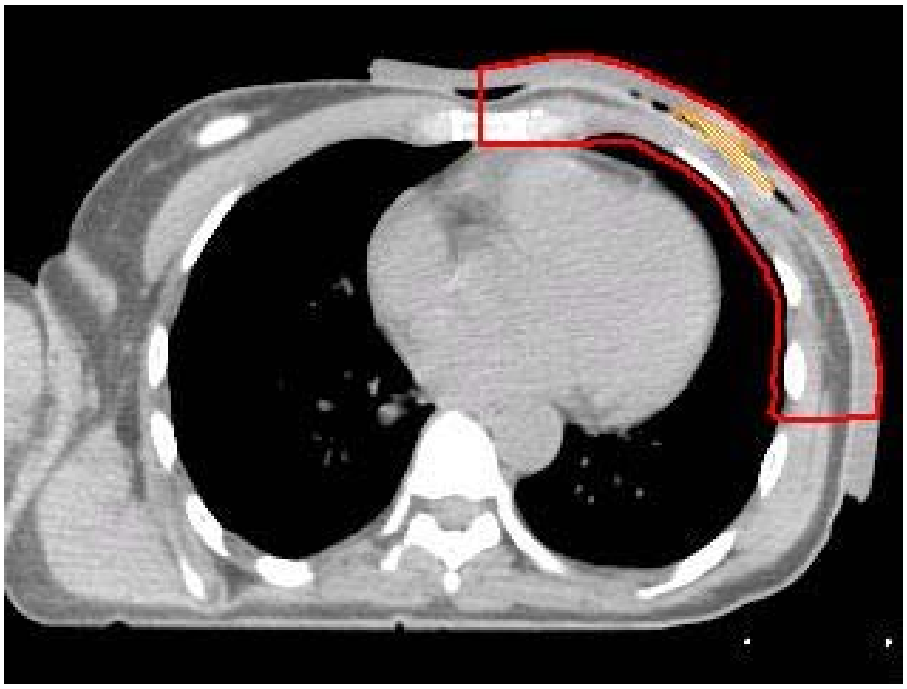

Figure 2.3. PTV is contoured in red line. Scar is shown in orange area.

The TomoTherapy TPS was used to generate an IMRT plan for each patient. The doseprescription was 50 Gy in 25 fractions (200 cGy/fraction) for all patients. All treatment plans in this study were performed by a board certified dosimetrist (Eddie Singleton,CMD) to

reduce planning variations. The plan parameter values used for treatment planning were: field width = 2.45 cm; pitch = 0.287, planning modulation factor = 3.00, dose grid resolution = 'normal'

E. Characterizing Intrafraction Chest Wall Motion

To characterize intrafraction chest wall motion over all phases of the patient's breathing cycle, each CT-SPOT® pellet placed during 4DCT scan was analyzed for maximum movement in the medial-lateral, anterior-posterior, and superior-inferior direction. In Pinnacle, the pellets placed around the patients mastectomy scar were identified on each phase image set of the 4DCT, and a POI was added at the location for each pellet. A sample 3D skin rendering showing the skin surface POIs and scar is shown in Figure 2.4(a). A photo showing the actual marker and scar position at the time of CT acquisition is shown in Figure 2.4(b) for comparison.

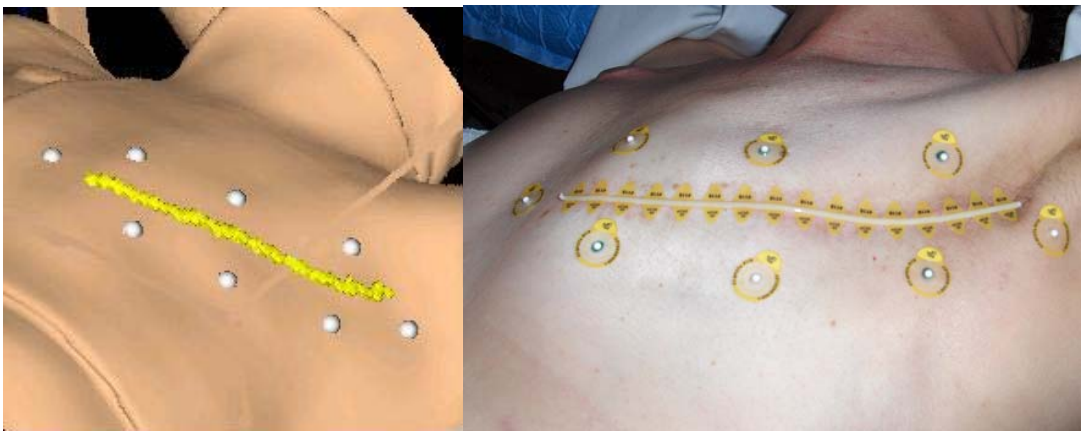

(a) (b)

Figure 2.4. Image (a) of 3D skin rendering showing POIs as white dots on skin surface. Scar contoured and shown in yellow. Picture (b) of the actual CT-SPOT® pellet placements on patient.

Figure 2.5 shows the 3D skin rendering of 5 patients (A-E) with 6 to 8 different colored spheres representing the placement of radiopaque pellets taped prior to their scan. The spheres are for visualization purposes and not to scale. Mastectomy scars are shown in purple.

Once a POI was added, its location in the AP, SI, and lateral directions was located in the CT coordinate system. Figure 2.6 shows the sample location of a single marker at each phase of

the breathing cycle. The arrow points to the marker and the CT coordinates are shown in the lower left corner of each image.

To numerically analyze marker movement, the coordinate at each phase was recorded. For each pellet, the maximum separation was determined from the maximum spread of each coordinate over all ten breathing phases. The overall intrafraction chest wall motion of each patient was taken to be the largest marker displacement over all phases of breathing.

II. Aim 2

Aim 2 was to analyze clinical CW dose data at multiple points during treatment for comparison with calculated dose. CW point doses measured with TLD for 5 TomoTherapy PMRT patients (Patient A-E). TLD measurements were repeated every fraction for the first week then every other fraction after that to collect 15 data sets total. Their mean region of interest (ROI) dose was obtained from Pinnacle TPS and the TLD measured dose was compared to the calculated dose. A treatment verification MVCT scan was acquired prior to the daily treatment and their data was transferred to Pinnacle TPS to study the air cavity created between bolus and the CW surface.

A. Chest Wall TLD Measurements

1. Measurement Conditions

Each TL dosimeter contained LiF TLD-100 powder sealed in a cellophane packet. Each packet contained approximately 45-mg of powder in an approximately 1 x 1 x 0.2 cm^3 volume, spread to create an approximately even layer. Of the multiple pellet points used to evaluate chest wall motion, 3-4 locations were selected as TLD positions to measure delivered dose. For some patients, an additional TLD mark was added at the midpoint of the scar on the first day of the treatment. Setup photos showing the location of the TLD placement were taken and compared visually to 3D rendering images obtained from Pinnacle TPS and shown in Figure 2.7-2.11.

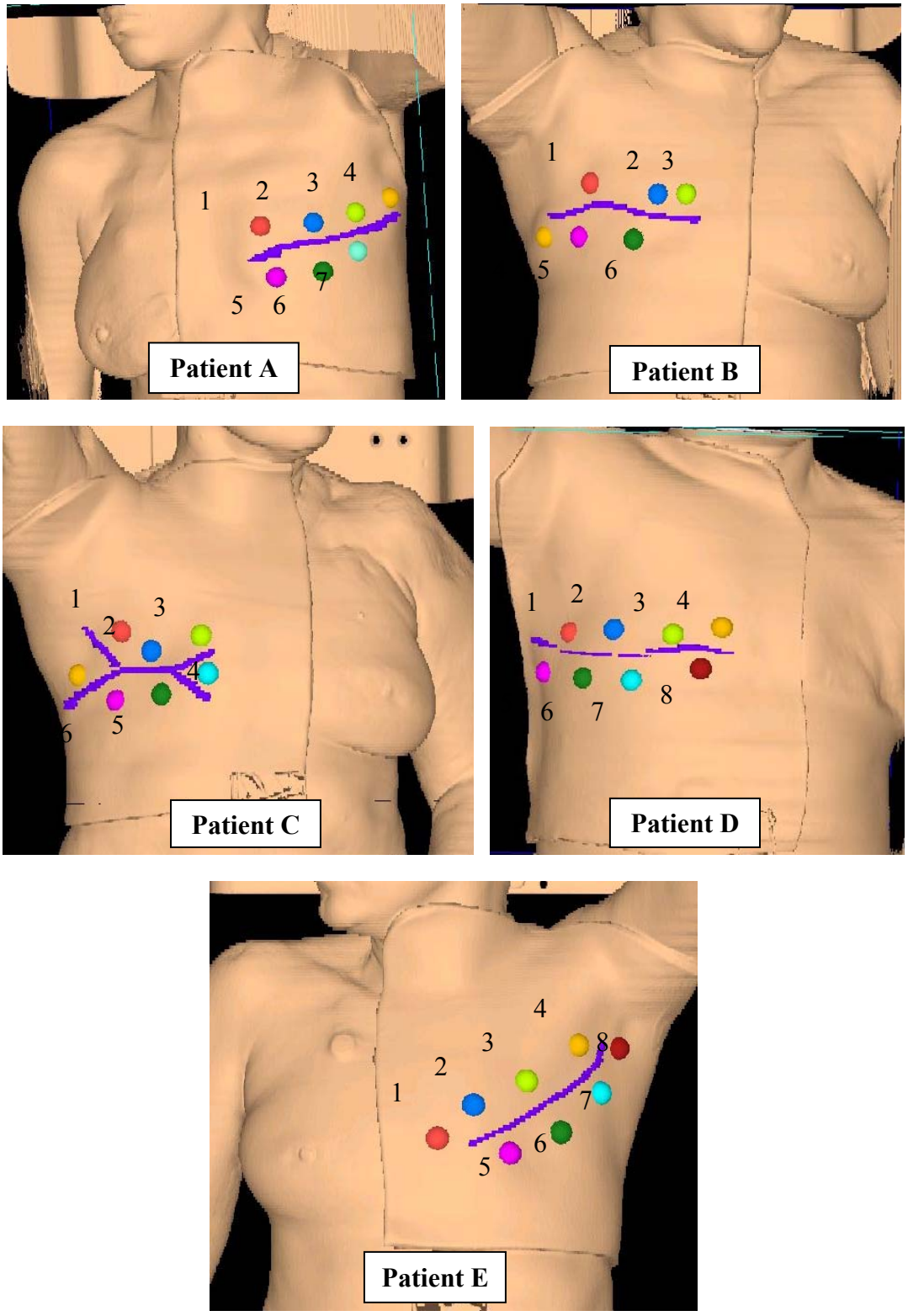

Figure 2.5. 3D skin rendering images of patients A through E with 7-8 spheres representing the location of radiopaque markers displaced on surface.

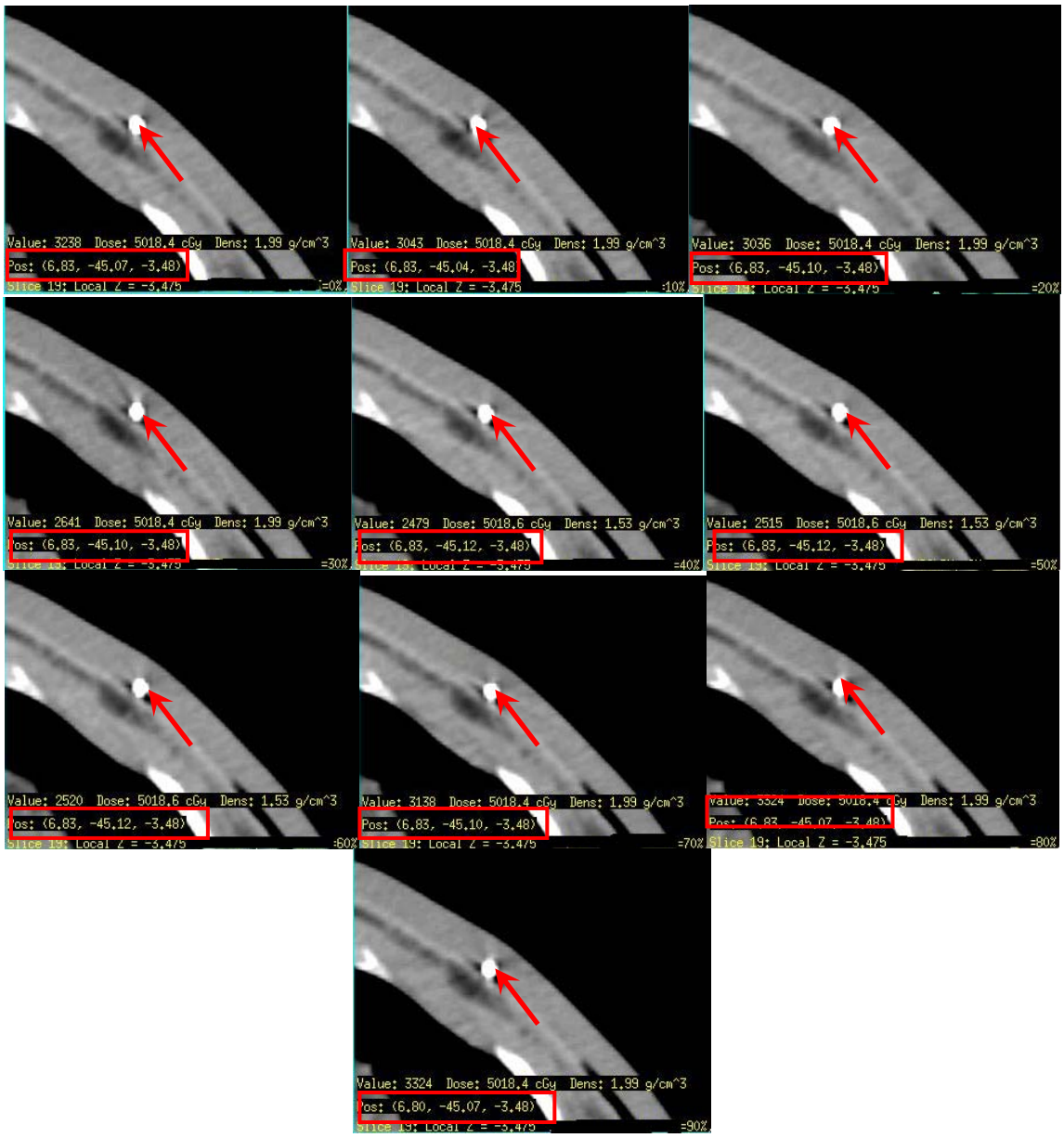

Figure 2.6. Tracking of the marker movement at each stage of breathing cycle and their coordinate recorded.

2. Patient TLD Irradiation

At the beginning of the each daily treatment, prior to MVCT scan, one TLD packet was taped on each mark. Then, patients were aligned to their reference marks and the bolus was placed on the chest wall. Each daily MVCT scan was performed using coarse slice thickness (6 mm) to reduce the scanning time. Once the MVCT image was acquired, the image registration to the planning CT images was performed. Initial registration was performed using TomoTherapy's

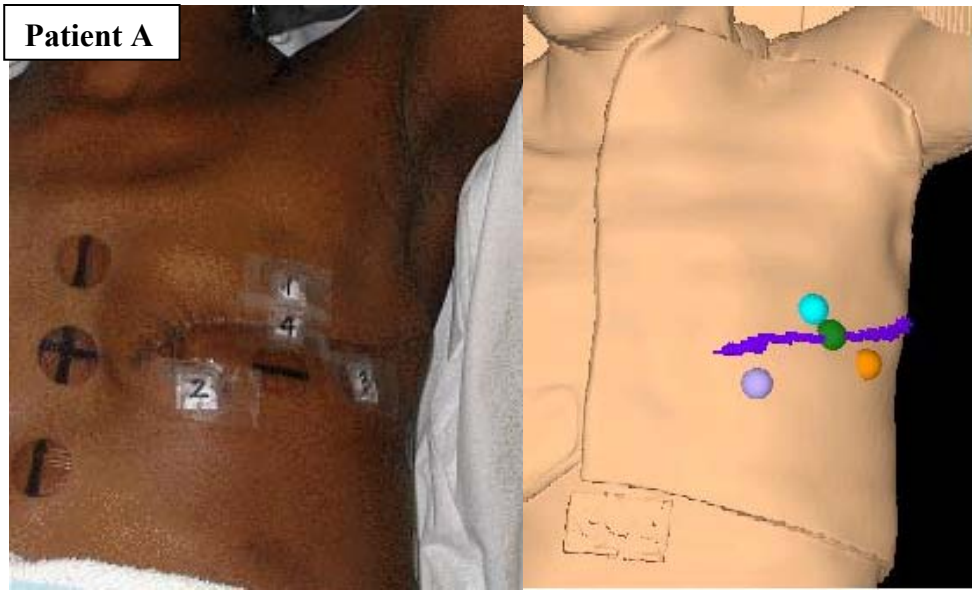

Figure 2.7. Placement of In-vivo TLDs for Patient A: (a) Patient photo showing the location of the TLD placement and (b) 3D rendering image of the same patient from Pinnacle TPS.

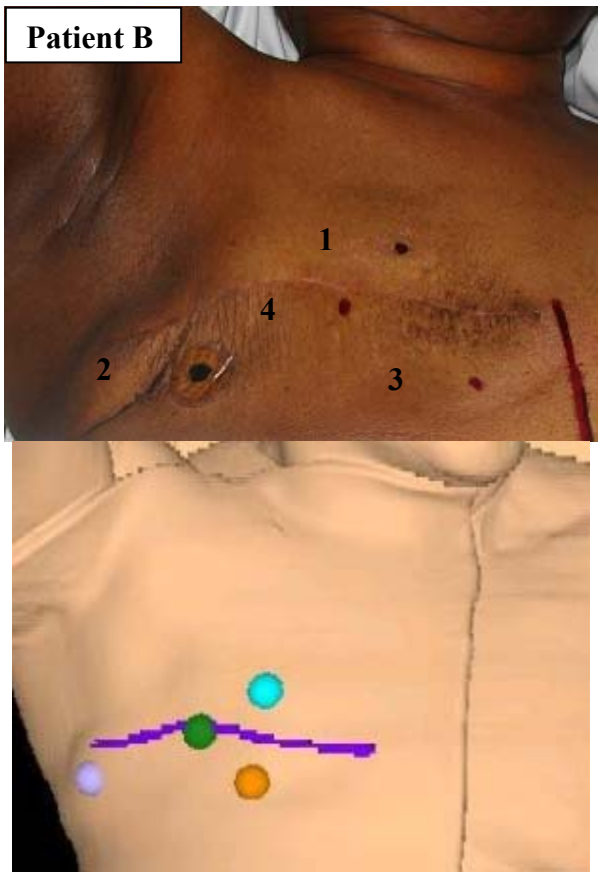

Figure 2.8. Placement of In-vivo TLDs for Patient B: (a) Patient photo showing the location of the TLD placement and (b) 3D rendering image of the same patient from Pinnacle TPS.

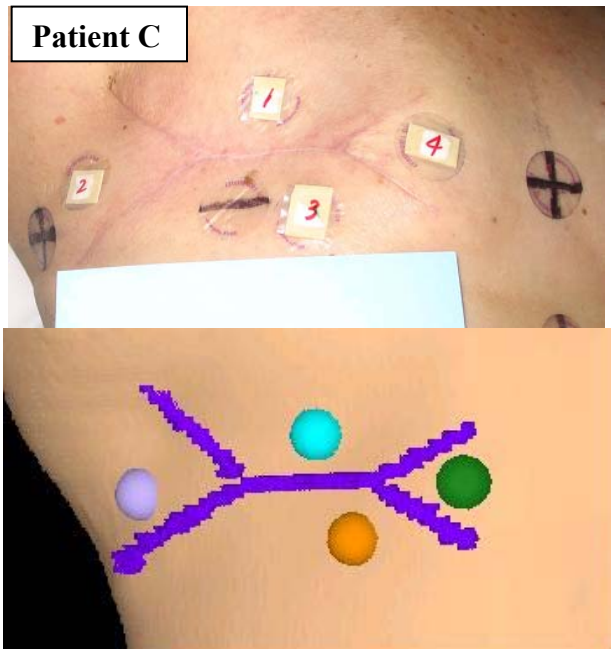

Figure 2.9. Placement of In-vivo TLDs for Patient C: (a) Patient photo showing the location of the TLD placement and (b) 3D rendering image of the same patient from Pinnacle TPS.

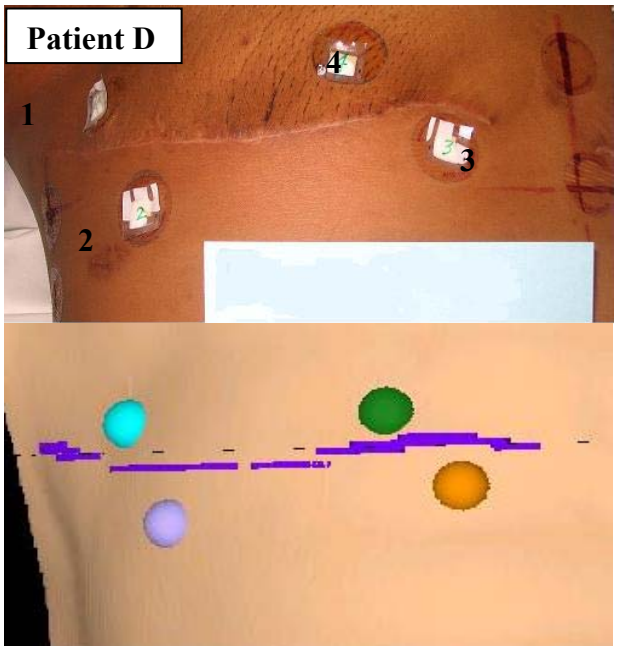

Figure 2.10. Placement of In-vivo TLDs for Patient D: (a) Patient photo showing location of the TLD placement and (b) 3D rendering image of the same patient from Pinnacle TPS.

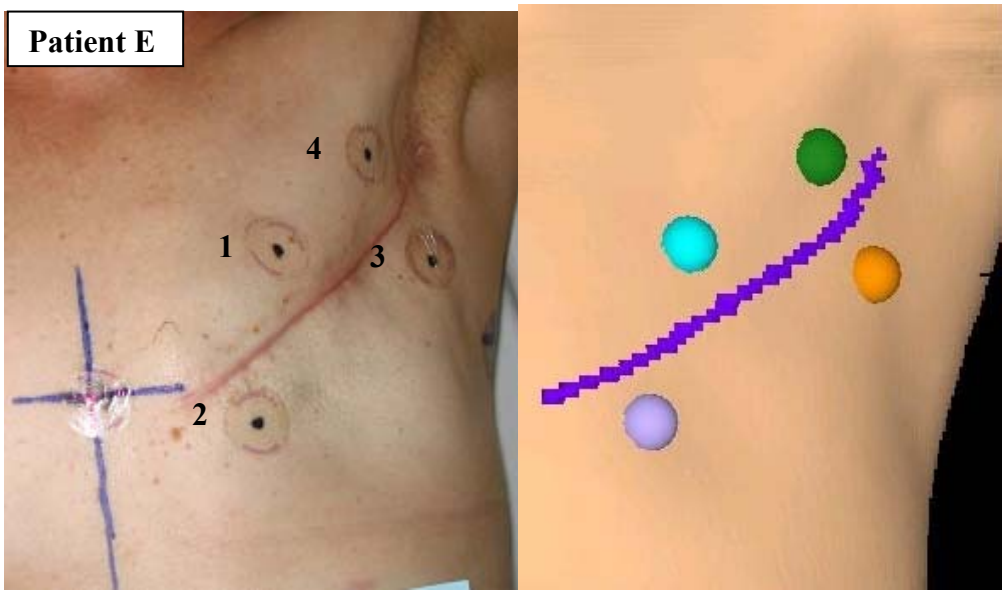

Figure 2.11. Placement of In-vivo TLDs for Patient E: (a) Patient photo showing location of the TLD placement and (b) 3D rendering image of the same patient from Pinnacle TPS.

automatic registration software. After that, the registration was manually adjusted giving preference to particular regions of interest (e.g., PTV). Additionally, the dose distribution (calculated on the planning CT data, not the daily MVCT) was evaluated to ensure adequate coverage of the PTV. Once the final registration was accepted, patients were re-positioned based on their calculated shifts and treatment was delivered. Once the treatment was completed, the bolus was removed and the TLD packets were collected for readout.

3. TLD Calibration

Calibration TLD packets were irradiated to known doses (100, 150, 200, and 250 cGy) that encompassed the expected daily fraction dose of 200 cGy. The TLDs were placed at 100 cm SSD at a depth of 1.5 cm in Plastic Water® on a Novalis BrainLab 6MV beam. Ten centimeters of Plastic Water® was used beneath the TLD packets to provide backscatter. One packet was not irradiated to determine the background signal. All the TLD packets were kept in dark over night to be read the next day. TLD's were calibrated every day and used to determine the measured dose for the clinical TLD's irradiated on that same day. This was done to minimize effects of

time between exposure and readout since the time difference (approximately 24 hours) was approximately the same for the calibration and experimental TLD's each day.

4. Reading of TLDs and Conversion to Dose

The TLD samples were read using a REXON UL-320 Reader (Rexon Components, Inc.). An analytical balance (AL54, Mettler-Toledo, Inc.) was used to measure the mass of each powder sample that was read. The TLD powder in each packet was divided into 3 approximately equal samples (≈15mg each) to reduce uncertainty in the mean TL and thus dose value. The empty planchet was placed on a scale and weighed, then the balance was rezeroed to remove the planchet mass before the measurements were taken. For each sample, the thermoluminescence (TL) or the photon count from the peak of the glow curve (135°C to240°C) was recorded along with the mass of sample, allowing determination of $(TL/mass)_{sample}$. A net TL per mass, $(TL/mass)_{net}$, was found by subtracting the mean TL per mass of the background TLD sample, $(\overline{TL/mass})_{bkg}$, from the TL per mass of the sample, $(TL/mass)_{sample}$.

The calibration curve was obtained by determining the $(TL/mass)_{net}$ for each of the calibration doses. Sample TLD calibration data and fit is shown in Figure 2.12. For each calibration dataset, a linear fit was applied to the data, and sample doses were determined using the fit curve. Extrapolation was not needed, as the range of calibration doses encompassed the range of measured patient doses. The three samples of each packet were used to determine the mean dose and standard deviation of the mean for each TLD packet.

B. Obtaining Calculated TLD Doses

The TomoTherapy dose plan was exported to the Pinnacle TPS for determination of the calculated TLD doses. A region of interest (ROI) was added for each TLD packet at its location on the patient, as identified by the pellet's in the CT scan. The CT slice containing the center of

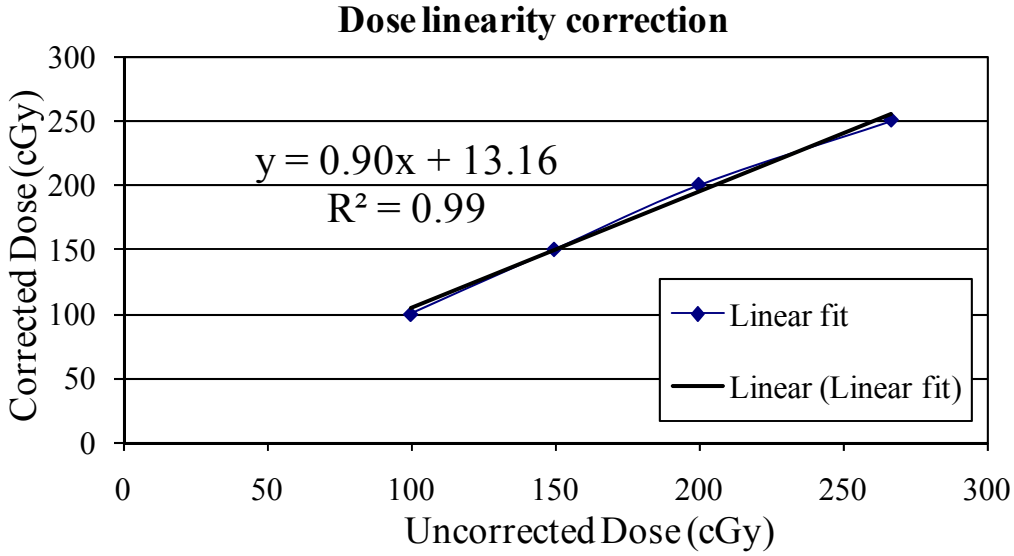

Figure 2.12. Sample TLD calibration data and fit

each pellet was located, and an ROI approximately 0.1 x 1 cm^2 was drawn centered on the pellet and on the surface of the chest wall, as seen in Figure 2.13(a). The ROI was copied to next two slices superiorly and inferiorly to approximate the physical size of the TLD packet. Average ROI dose was then obtained and compared to TLD measured doses. A sample TLD ROI and its dose statistics are shown in figure 2.13(b).

C. Evaluation of Effect of Air Cavity on Delivered Dose to Skin Surface

Correlation between the amount of air cavity created between thermoplastic bolus and the chest wall dose measured with TLD was analyzed and studied for the patients.

1. Importing MVCT Data to Pinnacle

TomoTherapy Hi-ART® planned adaptive software (Version 2.2.1.55) was used to retrieve daily MVCT images of the patients and export the data to Pinnacle. MVCT images were then compared with planning CT images to determine the location of the marker used for TLD placement. MVCT window and level were changed to default lung setting so that the air cavity between bolus and skin was clearly seen. Coarse resolution (6 mm slice thickness) was selected at the time of MVCT for all the CW patients. A POI was added at the location of each TLD.

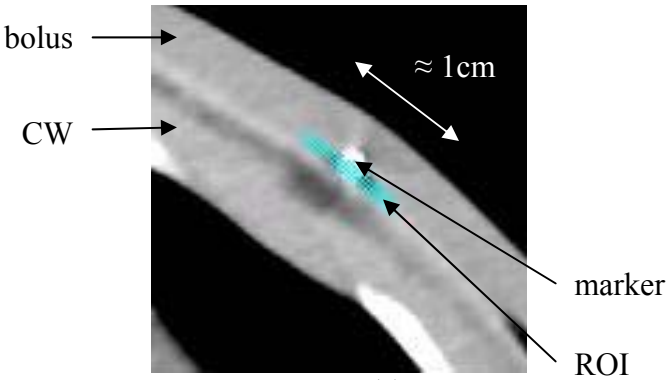

(a)

ROI Statistics

Line Type	ROI	Trial	Min.	Max.	Mean	Std. Dev.	% Outside Grid	% > Max
◆ —	TLD_1	Trial_1	5011.9	5264.8	5098.8	48.9	0.00 %	0.00 %

(b)

Figure 2.13. Sample TLD (a) ROI and (b) dose statistics. Mean ROI dose was used as calculated dose for a comparison.

placement. MVCT window and level were changed to default lung setting so that the air cavity between bolus and skin was clearly seen. Coarse resolution (6 mm slice thickness) was selected at the time of MVCT for all the CW patients. A POI was added at the location of each TLD.

2. Contouring of Air Cavity

Air cavities between the bolus and the patient's CW were contoured to obtain the air volumes surrounding the TLD pack. The amount of air volumes obtained were used to study the impact of air cavity on the chest wall doses. Air cavities within 2.5 cm of the TLD location were manually contoured and the total volume was obtained as shown in Figure 2.14. The thickness of the air cavity directly above the TLDs of air cavity above the TLD's were also measured and recorded to study the correlation between air cavity size and chest wall dose. Air contours were performed for the five patients (A through E) as well as for the Patient 3 (Patient F) from our preliminary patient data set, whose average difference between the calculated and prescribed

doses was 8.7%. Correlation between the air volume as well as air thickness above TLD packet, and TLD measured chest wall dose analyzed for data from the patients.

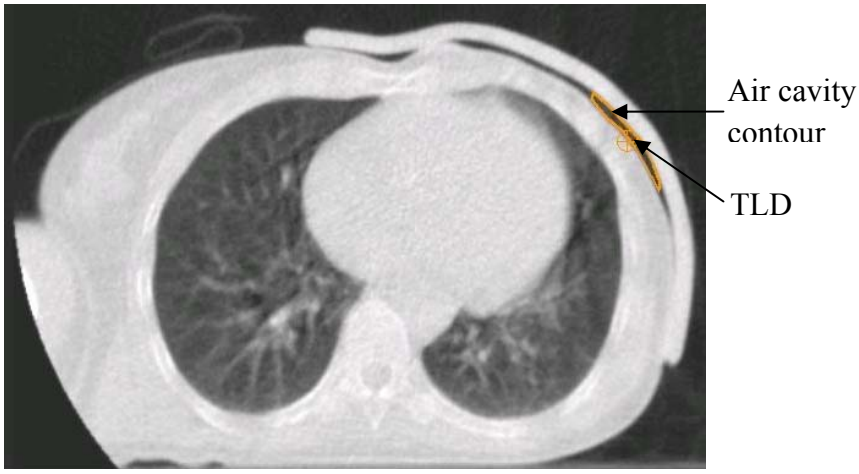

Figure 2.14. MVCT image of patient CW with bolus placed. TLD location in orange circle and air cavity contour in orange line is shown.

III. Aim 3

Aim 3 was to measure surface dose at multiple points on phantom and compare with calculated dose. 3 TLD measurements were performed to add confidence in our TLD measurements and their comparison to the calculated dose in both patient measurements and phantom measurements. Effect of phantom shift on delivered dose to surface and effect of foam cavity between bolus and the phantom surface on phantom surface dose were evaluated by using anthropomorphic CW phantom and compared with patient data.

A. TLD Measurements Test

1. Accuracy and Precision of TLD Measurements Due to TLD System

Measurements to test the accuracy and precision of our TLD system used in this study were performed. Three independent sets of measurements were taken to obtain the accuracy of our TLD system. Each experimental set of TLD's were irradiated to 175, 200, and 225 cGy using the same geometry as the calibration TLD on the conventional linac. All the TLD packs were

read and the TLs were converted in doses the next day. Predicted and measured doses were then compared.

2. Accuracy of TLD Dose Measurements in Anthropomorphic CW Phantom

The accuracy of patient measurements depends primarily upon accuracy of TLD system, accuracy of TomoTherapy delivery, accuracy of the TomoTherapy treatment planning system, intrafraction patient motion, how well the bolus fits the patient, and possibly other patient-dependent factors. As the present study is designed to evaluate dose inaccuracies due to patient effects, the present section looks at dose accuracy without such patient effects. This is done by comparing measured with calculated dose for an anthropomorphic Torso Phantom™ (Spect company info. Model ECT/TOR/P), shown in Figure 2.15(a)-(c).

The phantom included large, body-shaped lung, liver and spine inserts. Lung inserts were filled with Styrofoam® beads and water to simulate average lung tissue density. The liver insert, and remainder of the phantom except spine insert was filled with water. Lateral (R-L) and anterior-posterior outside dimensions were 38-cm and 26-cm, respectively, to simulate the upper torso of average to large male and female patients. The phantom wall thickness was 9.5-mm polymethylmethacrylate (PMMA).

a. Acquiring CT Scan

A scan of the phantom was acquired using the GE LightSpeed RT. To replicate clinical PMRT as closely as possible, mastectomy scar tape was placed laterally on the right CW surface. 4 CT-SPOTS® pellets (one superior, two inferior, and one in the middle of the scar) were placed, and locations of the pellets were marked using permanent marker for later placing the TLD prior to treatment delivery (c.f., figure 2.16).

The phantom was positioned on the couch so that the CT alignment laser would intersect the center of the phantom. CT-SPOTS® pellets were placed at the three laser alignment marker

(cross-hair), one on anterior and two laterals, as indicated by the crosshairs in Figure 2.16. Superflab plastic bolus (Company info.) was used instead of the clinical thermoplastic bolus to minimize air cavities between the bolus and phantom surface, which could affect the measured dose. Superflab bolus was placed on the phantom as shown in figure 2.17 and a CT scan was acquired with a 1.25-mm slice width. Images were transferred to Pinnacle TPS for contouring and to the TomoTherapy TPS for

treatment planning.

b. Planning ROIs

The Pinnacle TPS was used to contour ROIs (e.g., PTV and organs at risk, OARs). The PTV was drawn to cover the bolus and chest wall and to protrude into lung by more than 5 mm. OARs included lung, heart, spinal cord, and liver. Lung was contoured using Pinnacle's auto contour tool which uses CT thresholds. Since the phantom contained no heart insert, heart contours had to be drawn manually by comparing with patients image of similar anatomy. Figure 2.18 shows a CT slice with PTV contours in red, lung in green, heart in purple color wash, and spine in brown color wash. All the ROIs contours were evaluated and approved by a radiation oncologist prior to treatment planning.

ROIs were then transferred from the Pinnacle workstation to the TomoTherapy TPS. The TomoTherapy TPS was used to generate an IMRT plan for the phantom. It was planned according to clinical procedures described in previous section. The temporary dose distribution file (EOPDose.img) was saved along with the header file into a separate directory on the TomoTherapy workstation and subsequently exported to the Pinnacle workstation.

c. TLD Measurements

Repeated CW surface dose measurements using the TLD system were taken on the anthromorphic CW phantom. One TLD pack was taped on each mark on the phantom surface

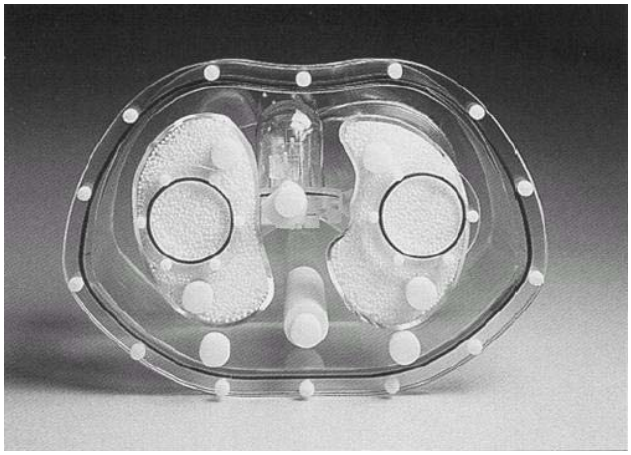

(a)

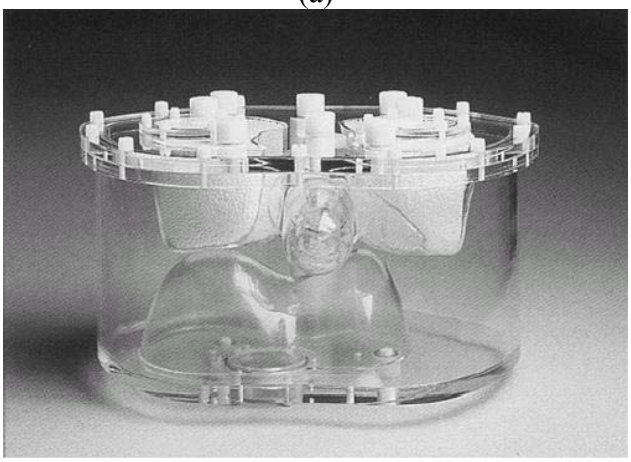

(b)

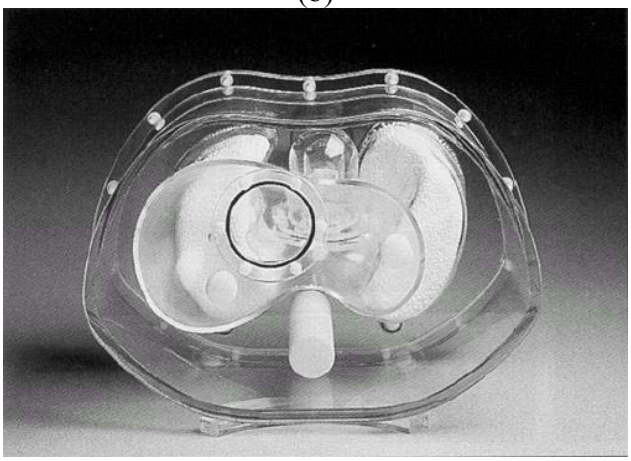

(c)

Figure 2.15. Pictures of (a) superior view, (b) anterior view, and (c) inferior view of the anthropomorphic Torso Phantom™ .

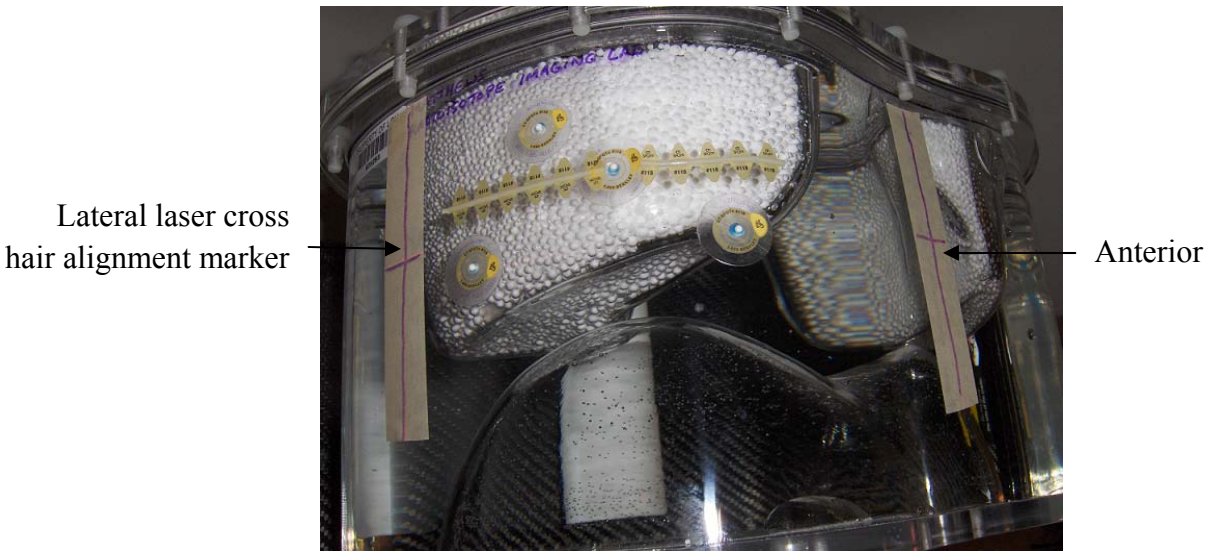

Figure 2.16. Picture of anthromorphic torso phantom with 4 pellets and scar tape. Bolus is not shown. Crosshair alignment marks are used to align phantom to isocenter lasers.

and 1 cm thickness Superflab bolus material was used to provide adequate buildup. The PMRT treatment plan was delivered and TLDs packs were collected. This measurement was performed one day and 3 times on other day. The packs were read along with that day's calibration TLD's and converted to dose.

To confirm our measurements, TomoTherapy Hi-ART® planned adaptive software (Version 2.2.1.55) was used to re-compute the dose distribution on the phantom based on the MVCT image data acquired prior to the treatment delivery for each set of the measurements. TLD measured dose was compared with (kVCT-based) and re-computed dose (MVCT-based).

3. Film Measurements

To improve confidence in our comparison between TLD measurements to calculation, the phantom surface dose was measured with Gafchromic® EBT film using the same setup as with the TLD measurements and compared with calculated dose and the previous measured TLD dose. They were not used as a mean of *in-vivo* dosimetry as the patient's CW's were more irregular than the phantom surface. An 8" x 10" film was taped onto the phantom surface to cover the

(a)

(b)

Figure 2.17. Pictures of anthromorphic torso phantom with superflab bolus in place: (a) right-anterior-inferior oblique view and (b) inferior view.

PTV as shown in Figure 2.19(a). The orientation of the film was recorded to be used for the image registration. The exposure included the MVCT scan and the treatment delivery. The measurement was repeated twice. A calibration film was exposed on the same 6MV linac as that used for the TLD calibration. The films were scanned the next day and the location of the TLD marks were identified by performing a geometric comparison. An image of the film with ruler tool identifying the TLD location is shown in Figure 2.19(b). The measured dose obtained at

each location was compared to the corresponding TLD measurement and the difference between the film measured dose to the calculation was then compared with the difference between calculation to the previous measured TLD dose.

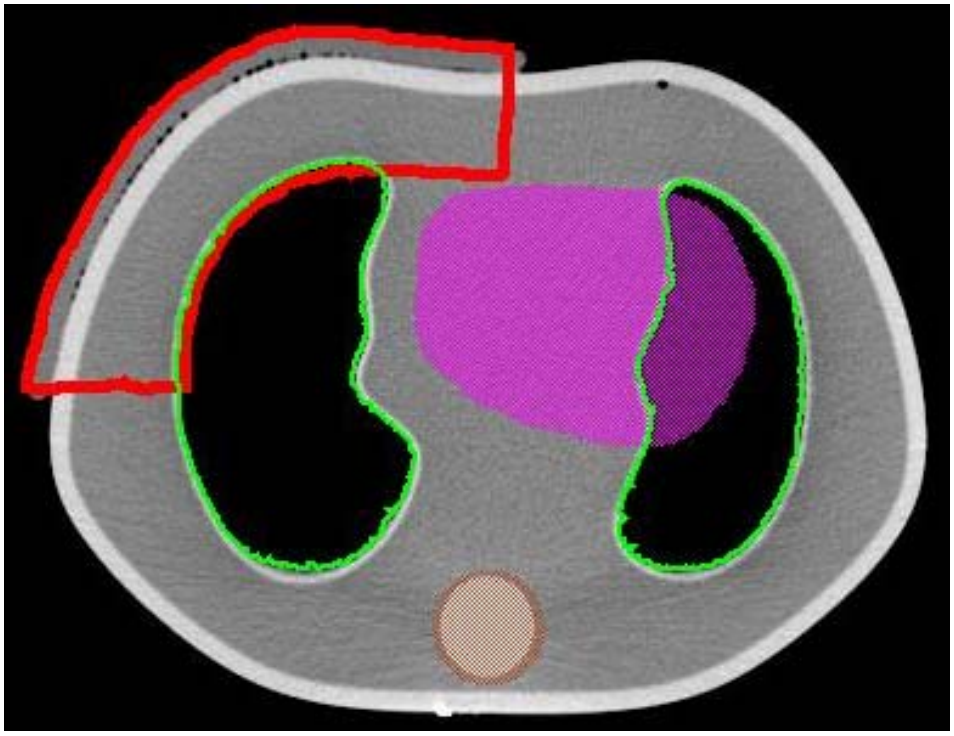

Figure 2.18. ROI contours. The PTV is shown in thick red contour, lungs are shown in green, spinal cord is shown as brown color wash, and heart is shown as purple color wash.

PTV as shown in Figure 2.19(a). The orientation of the film was recorded to be used for the image registration. The exposure included the MVCT scan and the treatment delivery. The measurement was repeated twice. A calibration film was exposed on the same 6MV linac as that used for the TLD calibration. The films were scanned the next day and the location of the TLD marks were identified by performing a geometric comparison. An image of the film with ruler tool identifying the TLD location is shown in Figure 2.19(b). The measured dose obtained at each location was compared to the corresponding TLD measurement and the difference between the film measured dose to the calculation was then compared with the difference between calculation to the previous measured TLD dose.

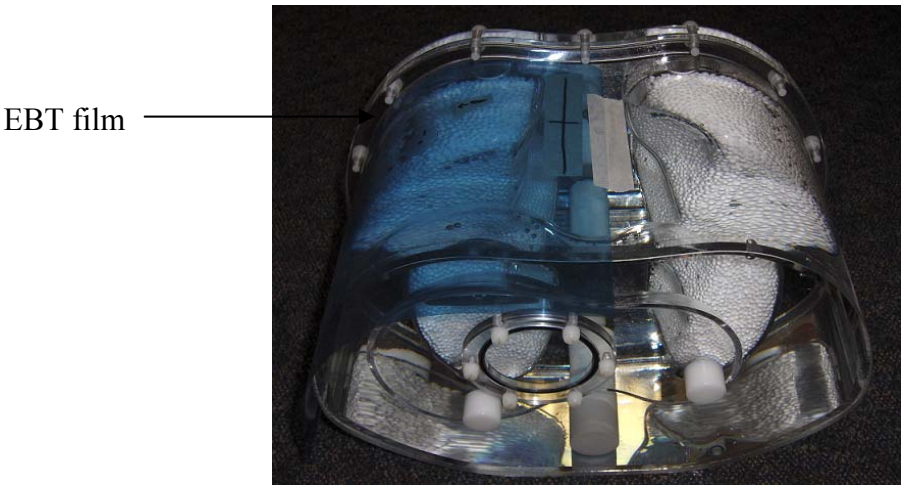

(a)

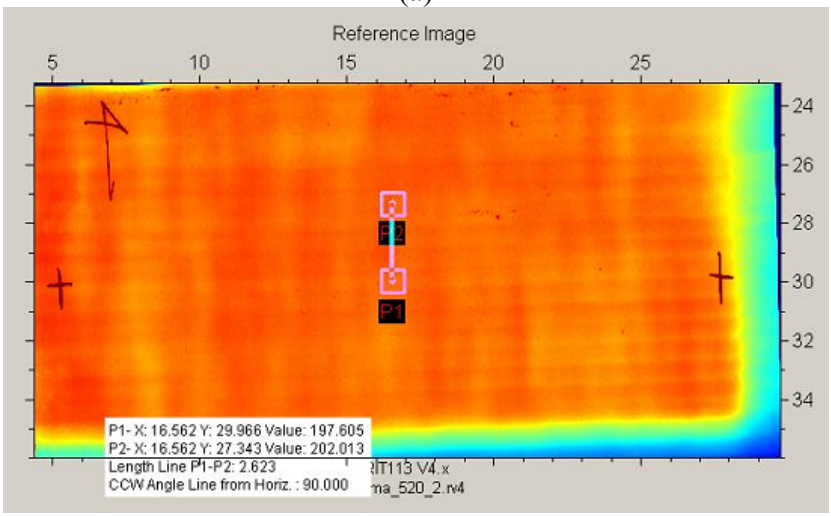

(b)

Figure 2.19. Picture of (a) the phantom with film taped and (b) image of the film converted to dose with ruler tool locating the TLD position.

B. Effect of Phantom Shift on Delivered Dose to Phantom Surface

The purpose of the following procedure was to estimate the maximum effect of intrafraction motion on dose delivery. After analyzing the patient's 4DCT data (explained in the previous section). It was determined that 1 cm AP chest wall motion would exceed any intrafraction movement expected from any PMRT patient. In fact, none of the five patient's intrafraction motion exceeded 1 cm. Based on these results, the physician included a 1-cm margin anteriorly on the PTV.

Three measurements were performed using the anthropomorphic Torso Phantom™ to evaluate the effects of a 1-cm position offset in a treatment delivery. The first measurement was made with the phantom in the treatment position specified in the treatment plan. Four TLD packages were taped on the phantom surface, and a 1-cm thick Superflab bolus was taped onto the phantom. A pre-irradiation MVCT scan which showed no shift was required to align the phantom prior to treatment. TLD packages were collected after treatment was delivered and kept inside the drawer away to avoid light exposure. The second and third measurements were made with a couch shift. The couch was shifted 1 cm posterior from its planned position for the second measurement and 1 cm anterior from its planned position for the third measurement. Figure 2.20(a) shows a setup photo of the phantom on TomoTherapy treatment couch and an illustration of couch shift is shown in Figure 2.20(b). The phantom remained stationary during the delivery as this was not a moving phantom study. 4 TLD packages and the bolus were placed on the same location for all the measurements. The experimental TLDs were read along with the calibration TLD set the next day. The results from the three measurements were compared and analyzed.

C. Evaluation of Effect of Air Cavity on Delivered Dose to Phantom Surface

Correlation between the amount of air cavity created between thermoplastic bolus and the chest wall dose measured with TLD was analyzed and studied for phantom measurements.

1. Measurement of Foam Density and Thickness

An evaluation of the effects of air cavities on surface dose required a way to accurately control the air cavity under measurement conditions. Superflab was used as the bolus material in this study to eliminate air cavities between the chest wall and bolus. These air cavities are common when using the thermoplastic bolus used clinically, as it tends to shrink and deform as it hardens over time. Additionally, changes in patient anatomy from that occurring in the planning CT data set can also create air cavities.

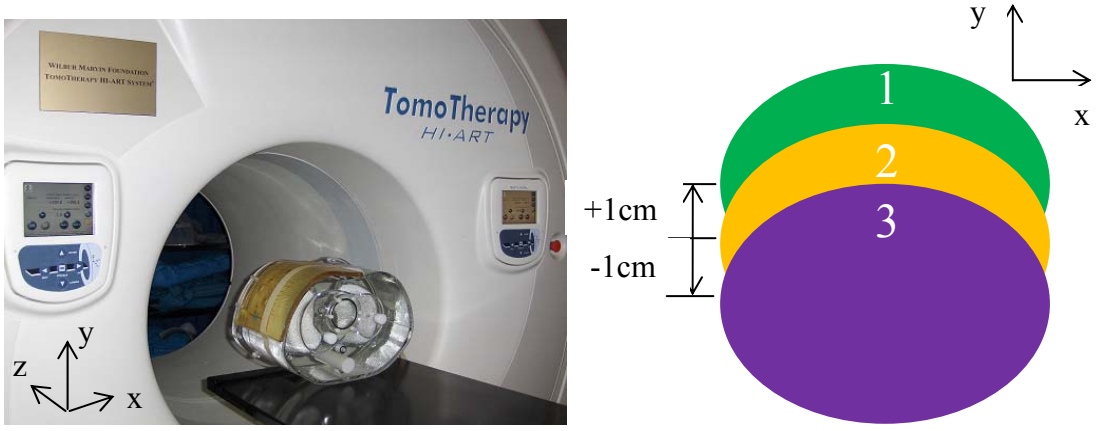

(a) (b)

Figure 2.20. (a) Setup photo of the phantom on TomoTherapy treatment couch, and (b) illustration of 1 cm couch shift phantom measurement.

To simulate air cavities in this study, a closed-cell foam packing material, cut into approximately 30x30x0.3 cm^3 sheets, was used. The average thickness, as well as the density of each packing material was determined by measurement. The thickness was measured with a KANON Vernier caliper. A Mettler Electronic Analytical Balance was used to determine the mass of each packing sheet, which were cut to have a 10 x 10 cm^2 cross section. Measurements were repeated 3 times to obtain uncertainty. The data, found in Table 2.1, showed a mean density of 0.0207±0.0014g cm^{-3}.

Table 2.1. Thickness and mass of foam cushioning material measured with the Vernier caliper and analytical balance respectively.

Foam Cushioning Material 10x10 cm^2 Measured Values

Sheet #	**Measured Thickness [mm] Vernier Caliper**	**Measured Mass [g] Analytical Balance**	**ρ[g cm^{-3}]**
1	2.98 ± 0.02	0.5753 ± 0.0001	0.0193
2	2.60 ± 0.02	0.5714 ± 0.0002	0.0220
3	2.78 ± 0.02	0.5791 ± 0.0002	0.0208
		Average	0.0207 ± 0.0014

2. TLD Measurements

The anthropomorphic phantom and plan used in the previous section were used to evaluate the effects of air cavities on delivered dose. Varying thicknesses of foam (0-18 mm in 3 mm increments) were placed and taped to the phantom. Superflab bolus was then placed on top of the air as shown in figure 2.21. MVCT images registrations were performed to align the phantom prior to the each treatment delivery. Once the treatment was completed, the bolus and the foam sheets were removed and the TLD packets were collected, read, and converted to dose. Correlation between the controlled air volume, as well as air thickness above the TLD packet, and TLD measured phantom surface dose were then analyzed.

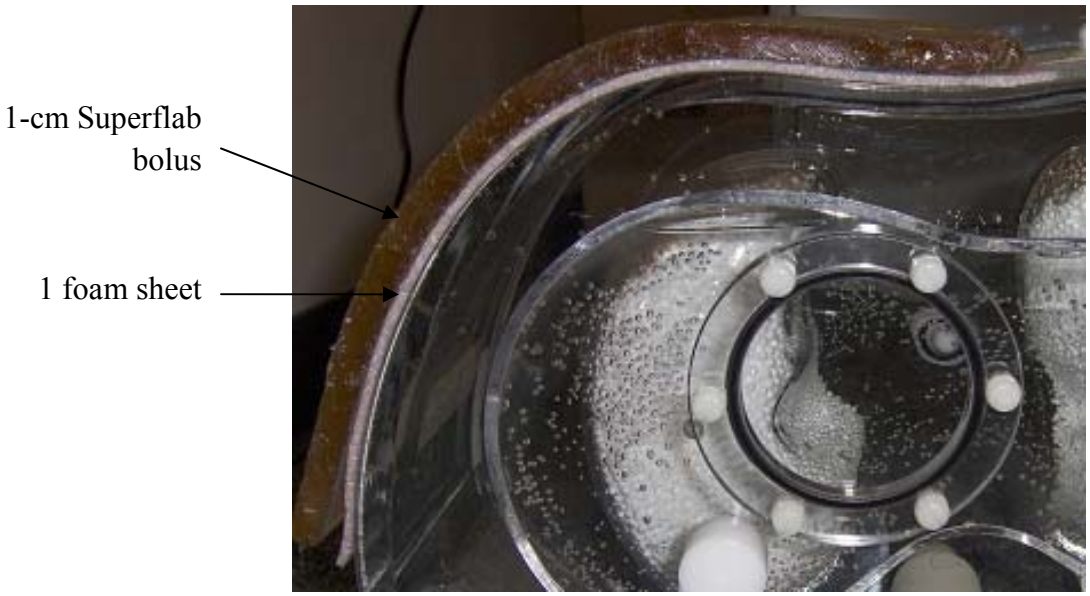

Figure 2.21. Foam cushioning material was placed between Superflab and phantom surface to simulate an air cavity

Chapter 3
Results

I. Aim 1

The results of intrafraction motion of radiopaque pellets for 5 patients are shown in Table 3.1a-e. 4DCT data showed small movements < 1.5mm in lateral and anterior-posterior (ant-pos) directions and less than 2.5mm in the superior-inderior (sup-inf) directions were observed for all patients and for each marker location. Since our study is on respiratory motion, ant-pos movement was of primary concern. Lateral movement was small at all TLD locations for all patients. The smallest lateral movement was 0.02 cm at Patient E locations 1 and 2. Sup-inf motion was either 0.25 cm or 0 cm as the CT slice thickness was 0.25 cm and the diameter of the marker was approximately 0.3 cm. The maximum patient chest wall motion data of all patients is shown in Table 3.1f. For each patient, the maximum displacement in each anatomic direction over all the markers was taken to be the intrafraction motion for that patient. Maximum ant-pos movements of patient A through E were 0.15 cm, 0.15 cm, 0.11 cm, 0.15 cm, and 0.06 cm respectively.

II. Aim 2

A. TLD Measurements

Results comparing the calculated to TLD-measured daily (fractional) doses at each TLD location for Patient A through E are shown in Figures 3.1 through 3.5. For each patient, dose was measured at four locations. For each TLD location, dose measurements are plotted versus fraction number for 15 of their 25 total fractions. Error bars represent the standard error of the mean for each dose measurement, which was obtained from three readouts of each TLD. The shaded region is the ±5% range about the calculated dose. Prescribed dose, calculated dose, average measured dose of each TLD, and the percent difference in measured and calculated

Table 3.1. (a) to (e) The results of intrafraction motion of radiopaque pellet markers for each patient. (f) A summary of our five patient's 4DCT data

(a) Patient A			
pellet Location	Lateral [cm]	Ant-Pos [cm]	Sup-Inf [cm]
1	0.1	0.09	0.25
2	0.05	0.15	0.25
3	0.04	0.14	0
4	0.09	0.07	0
5	0.03	0.11	0.25
6	0.06	0.08	0.25
7	0.06	0.14	0

(b) Patient B			
pellet Location	Lateral [cm]	Ant-Pos [cm]	Sup-Inf [cm]
1	0.1	0.09	0.25
2	0.05	0.15	0.25
3	0.04	0.14	0
4	0.09	0.07	0
5	0.03	0.11	0.25
6	0.06	0.08	0.25

(c) Patient C			
pellet Location	Lateral [cm]	Ant-Pos [cm]	Sup-Inf [cm]
1	0.04	0.07	0
2	0.07	0.07	0
3	0.07	0.07	0
4	0.07	0.07	0
5	0.1	0.07	0
6	0.07	0.11	0.25
7	0.08	0.11	0

(d) Patient D			
pellet Location	Lateral [cm]	Ant-Pos [cm]	Sup-Inf [cm]
1	0.04	0.08	0
2	0.08	0.13	0.25
3	0.08	0.15	0
4	0.03	0.11	0
5	0.04	0.14	0
6	0.12	0.09	0.25
7	0.08	0.08	0.25
8	0.08	0.12	0

(e) Patient E			
pellet Location	Lateral [cm]	Ant-Pos [cm]	Sup-Inf [cm]
1	0.02	0.04	0
2	0.02	0.03	0
3	0.03	0.04	0
4	0.05	0.06	0
5	0.05	0.08	0.25
6	0.06	0.05	0
7	0.03	0.06	0
8	0.03	0.06	0

(f) Maximum			
Patient	Lateral [cm]	Ant-Pos [cm]	Sup-Inf [cm]
A	0.09	0.15	0.25
B	0.1	0.15	0.25
C	0.1	0.11	0.25
D	0.12	0.15	0.25
E	0.06	0.06	0.25

calculated doses for each TLD location are shown for each of the 5 patients in Tables 3.2 through 3.6. Percent differences were obtained from the equation below:

$$\Delta(\%) = \frac{(Average\ Measured\ dose - Calculated\ dose)}{Calculated\ dose} \times 100\% \qquad (1)$$

Patient A had 3 packets of TLD taped around the scar and one at the middle of the scar (cf. Figure 3.1a). Differences between TLD measured and calculated doses for Patient A are plotted for each TLD in Figures 3.1b-e. Small variations in the measured dose were observed over the course of treatment, but 70% of the measured dose was within 5% of the calculated dose at all TLD locations. A summary of the comparisons is shown in Table 3.2, TLDs 1 and 4 were positioned adjacent to each other and both agreed well, being 1.5% low and 1.1% high, respectively. TLDs 2 and 3 were positioned medial, lateral and slightly inferior to TLDs 1 and 4 and slightly inferior. Their readings were 2.7% high and 3.7% low, respectively. Overall, results are well within the standard criteria for delivered dose accuracy of 5%.

Table 3.2. Prescribed, calculated, mean TLD measured dose, and Dose difference between calculated and measured doses of patient A.

	Prescribed Doses		**Calculated Doses**	**Measured Doses**		**Differences**
TLD	fxs [#]	fx Dose [cGy]	[cGy]	N	$D \pm \sigma_D$ [cGy]	$\Delta \pm \sigma_\Delta$ [%]
1	25	200	204	15	203.2 ± 5.3	-0.4 ± 2.6
2	25	200	210.5	15	216.1 ± 9.1	2.7 ± 4.3
3	25	200	206.7	15	199.1 ± 8.6	-3.7 ± 4.1
4	25	200	204.8	15	207.0 ± 8.1	1.1 ± 4.0

Patient B's TLDs were placed similarly to patient A's TLDs. TLD 1 was placed superior to the scar, TLDs 2 and 3 were placed lateral, medial and inferior to the scar, respectively, and TLD 4 was placed on top of the scar (cf. Figure 3.2b). Differences between TLD measured and

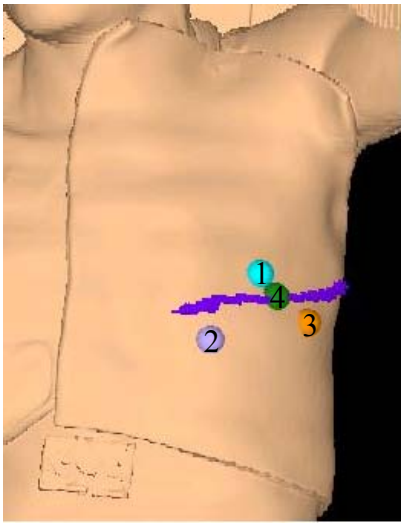

(a)

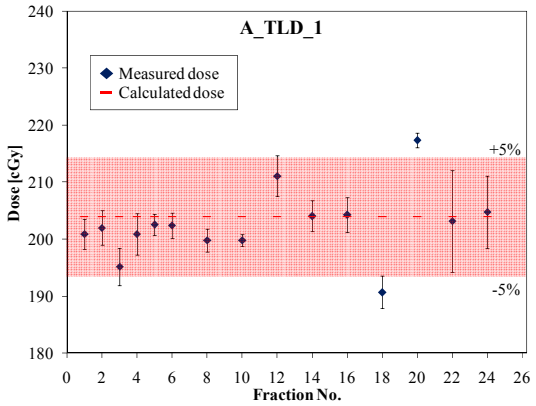

(b)

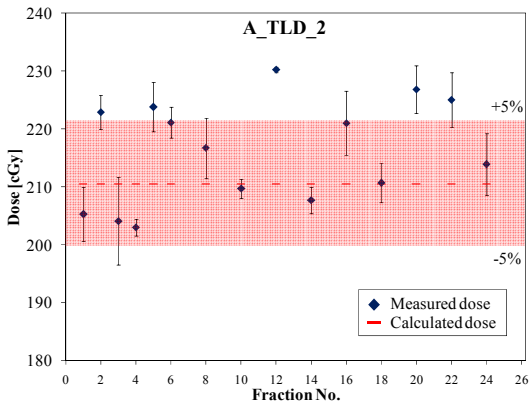

(c)

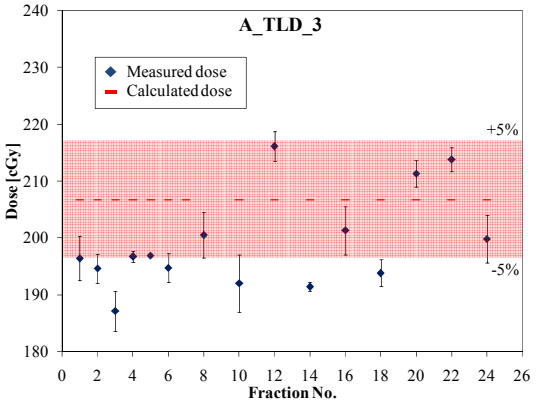

(d)

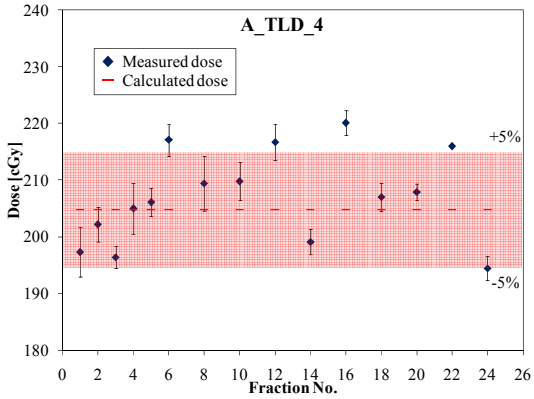

(e)

Figure 3.1. Patient A: (a) Picture of TLD placement and (b) through (e) Data comparing the calculated dose to TLD measured fractional daily dose at each TLD location. The pink region is the ±5% range about the calculated dose.

calculated doses are plotted for each TLD and shown in Figures 3.2b-e. 90% of measured TLD read lower dose than calculation and 63% of the difference exceeded than 5% at TLD 1 and TLD 3. A summary of the comparisons is shown in Table 3.3. Dose difference between calculated and TLD measured dose for TLD 1 and 3 that were positioned adjacent to each other, exceeded more than the standard criteria of 5 % (-5.4 % and -5.2%, respectively). TLD 2 and TLD 4 both agreed well, being 3.6% low and 2.4% respectively.

Table 3.3. Prescribed, calculated, mean TLD measured dose, and Dose difference between calculated and measured doses of patient B.

	Prescribed Doses		**Calculated Doses**	**Measured Doses**		**Differences**
TLD	fxs [#]	fx Dose [cGy]	[cGy]	N	$D \pm \sigma_D$ [cGy]	$\Delta \pm \sigma_\Delta$ [%]
1	25	200	199.9	15	189.2 ± 9.1	-5.4 ± 4.6
2	25	200	203.7	15	196.4 ± 5.4	-3.6 ± 2.6
3	25	200	199.8	15	189.5 ± 5.9	-5.2 ± 3.0
4	25	200	198	15	193.5 ± 4.6	-2.3 ± 2.3

A summary of the comparison is shown in Table 3.4 where TLDs 1 and 2 had -0.4% dose differences between calculated and measured dose and 1.6% and 1.7% differences were observed for TLDs 3 and 4, respectively.

Patient C had 4 packets of TLD taped to surround the scar, one superior, one inferior and two laterals (cf. Figure 3.3a). Differences between TLD measured and calculated doses for Patient C are plotted for each TLD in Figures 3.3b-e. Small variations in the measured dose were observed over the course of treatment, only 3 TLD fraction doses exceeded the calculated dose by more than 5%. A summary of the comparisons is shown in Table 3.4 TLDs 1 and 3 were positioned adjacent to each other and both agreed well, being 0.2% low and 1.7% high, respectively. TLDs 2 and 4 were positioned medial, lateral to the scar ends. Their readings were

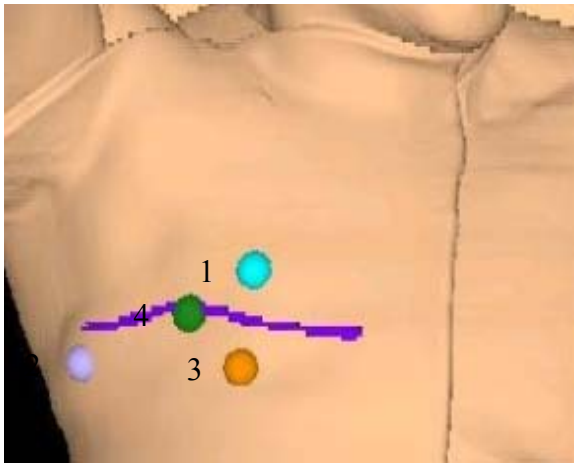

(a)

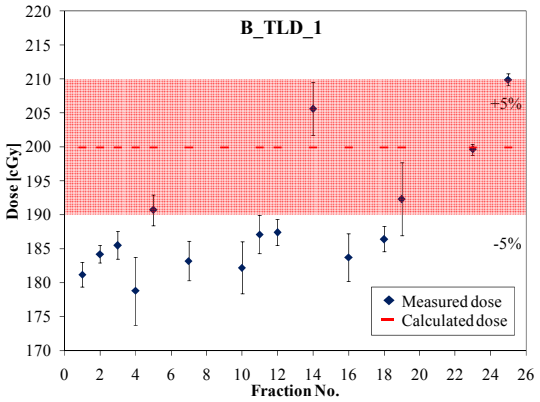

(b)

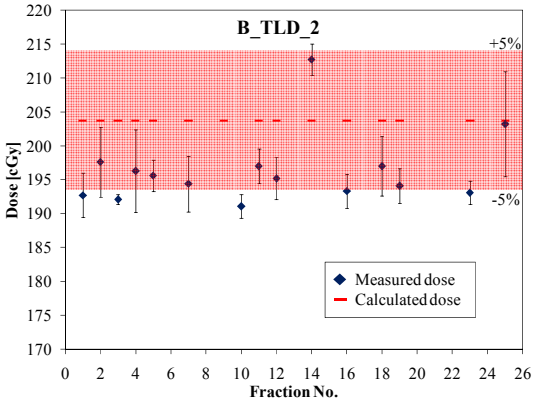

(c)

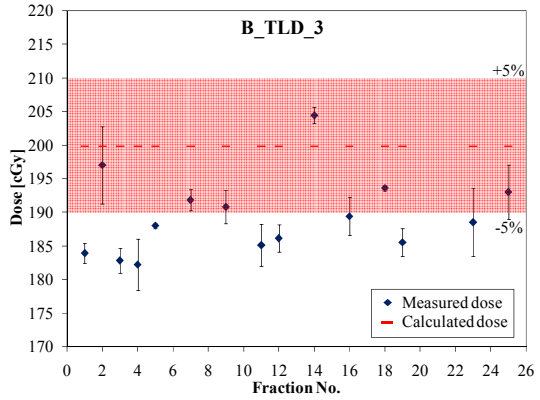

(d)

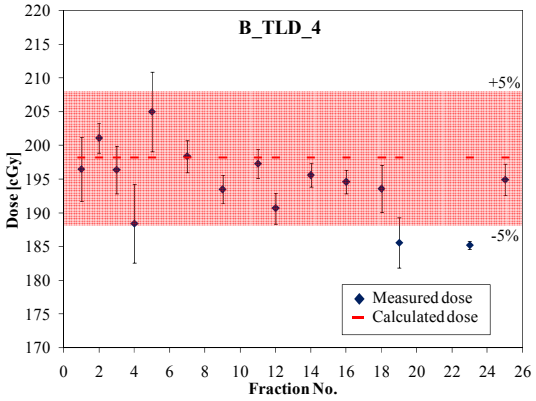

(e)

Figure 3.2. Patient B: (a) Picture of TLD placement and (b) through (e) Data comparing the calculated dose to TLD measured fractional daily dose at each TLD location. The pink region is the ±5% range about the calculated dose.

0.2% low and 1.7% high, respectively. Overall, results are well within the standard criteria for delivered dose accuracy of 5%.

Table 3.4. Prescribed, calculated, mean TLD measured dose, and Dose difference between calculated and measured doses of patient C.

	Prescribed Doses		**Calculated Doses**	**Measured Doses**		**Differences**
TLD	fxs [#]	fx Dose [cGy]	[cGy]	N	$D \pm \sigma_D$ [cGy]	$\Delta \pm \sigma_\Delta$ [%]
1	25	200	200.9	15	200.5 ± 5.6	-0.2 ± 2.8
2	25	200	202.4	15	201.9 ± 7.3	-0.2 ± 3.6
3	25	200	201.5	15	204.8 ± 7.0	1.6 ± 3.5
4	25	200	202.6	15	206.1 ± 5.6	1.7 ± 2.7

Patient D had 4 TLD packets placed to surround the scar as shown in Figure 3.4a. TLD measured fractional daily dose at each TLD location were plotted with calculated dose and shown in Figure 3.4b-e. 72% of measured TLD exceeded the calculated dose by more than 5%. But overall, the variation averaged out and the largest averaged difference out of four TLD locations at TLD 1 and 2 were -4.0%. A summary of the comparison is shown in Table 3.5 where TLDs 1 and 2 had -4.0% dose differences between calculated and measured dose and 2.2% and 3.4% differences were observed for TLDs 3 and 4, respectively.

Patient E had 4 TLD packets placed to surround the scar as shown in Figure 3.5a. Again, small variation of the measured dose was observed but 73% of the TLD doses were with within 5% of the calculated dose. A summary of the comparison between average measured to calculated dose is shown in Table 3.6. Difference of each TLD was -0.7%, -2.0%, -2.6%, and -3.3% for TLD 1, TLD 2, TLD 3, and TLD 4, respectively.

B. Impact of air cavity between bolus and the CW

The percent difference between calculated and measured doses were plotted against air cavity size to determine if the values were correlated. Dose differences were compared to both cavity thickness (at the location of the TLD) and cavity volume. Data was first divided into

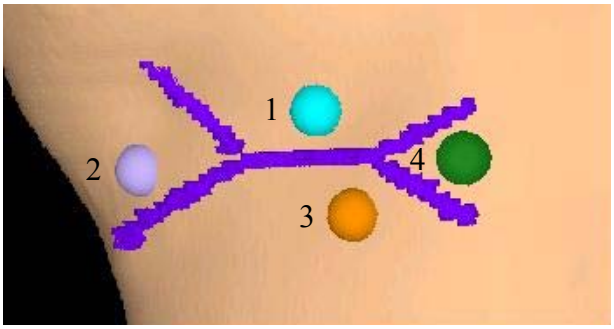

(a)

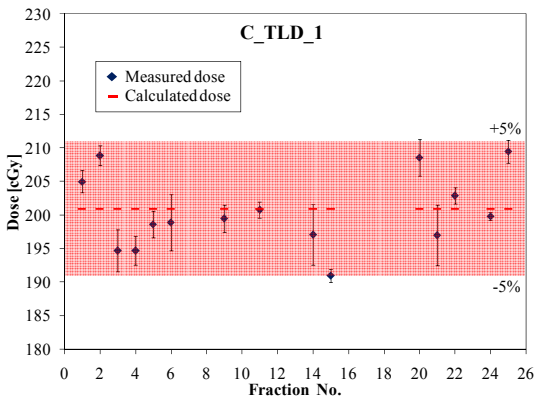

(b)

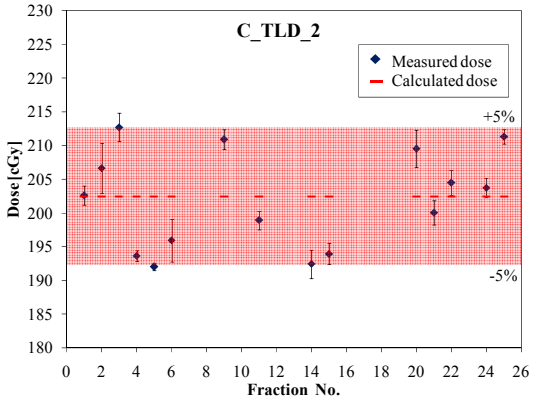

(c)

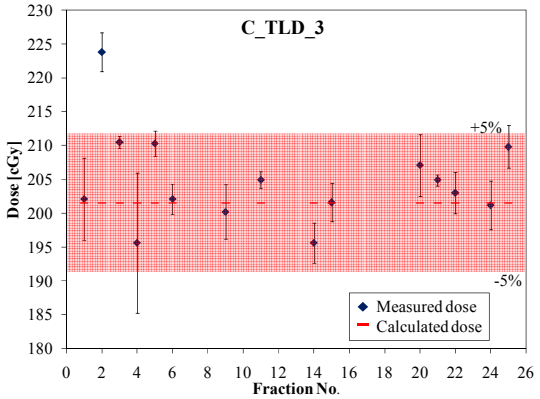

(d)

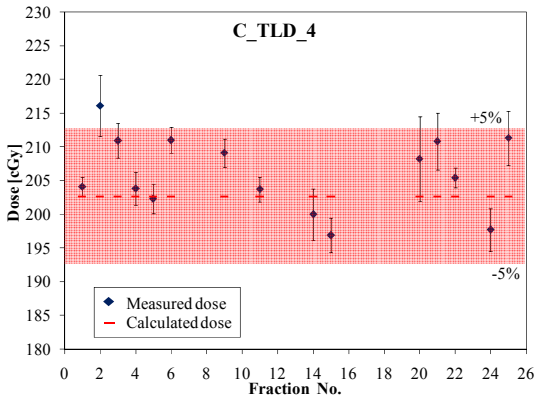

(e)

Figure 3.3. Patient C: (a) Picture of TLD placement and (b) through (e) Data comparing the calculated dose to TLD measured fractional daily dose at each TLD location. The pink region is the ±5% range about the calculated dose.

Table 3.5. Prescribed, calculated, mean TLD measured dose, and Dose difference between calculated and measured doses of patient D.

	Prescribed Doses		Calculated Doses	Measured Doses		Differences
TLD	fxs [#]	fx Dose [cGy]	[cGy]	N	$D \pm \sigma_D$ [cGy]	$\Delta \pm \sigma_\Delta$ [%]
1	25	200	201.2	15	194.1 ± 8.1	-3.5 ± 4.0
2	25	200	203.6	15	196.0 ± 8.4	-3.7 ± 4.1
3	25	200	204.5	15	207.3 ± 6.4	1.4 ± 3.1
4	25	200	205.7	15	210.8 ± 9.3	2.5 ± 4.5

individual TLD location 1-4, and then the percent difference between calculated and measured doses were plotted against air gap volume for patient A as shown in Figure 3.6(a)-(b). The slope for best-fit linear regression to all the data points for 4 TLD locations were 0.39, 1.1, 1.1, and 0.54 % cm^{-3}. R-squared values, goodness of fit, were 0.35, 0.16, 0.57, and 0.19. Slope and R-squared values of all the TLD locations combined result was 0.61 % cm^{-3} and 0.3. (Figure 3.7b). Because the R-square value for all TLD locations combined did not deviate from the individual divided data, the rest of the analysis was only done for each patient but not at each TLD location. The resulting plots are shown in Figures 3.7 to 3.11. Data for a preliminary TLD patient (Patient 3, figure 1.6c) whose result showed a downward trend of measured dose as the treatment progressed was analyzed as well and shown in Figure 3.12 as patient F and the patient A-E combined result is shown in Figure 3.13. The percent dose difference was determined using equation (2).

$$Dose\ Difference\ [\%] = \frac{(Calculated\ Dose - Measured\ Dose)}{Calculated\ Dose} \times 100\% \qquad (2)$$

Each patient had 60 data points (15 fractions × 4 dose points/fraction) to correlate the dose difference to the air cavity volume and thickness. Best-fit linear regression to all the data points is shown on the plots along with the equation and R-squared value. Scales were kept the same for

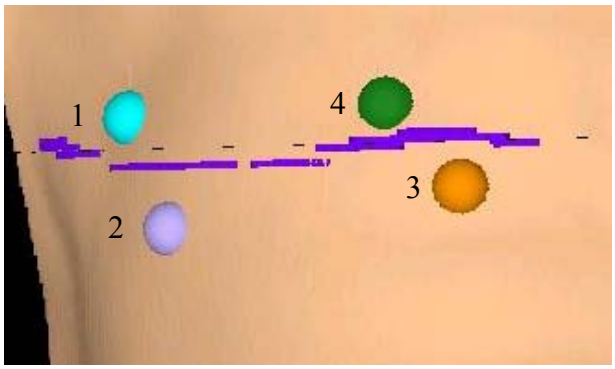

(a)

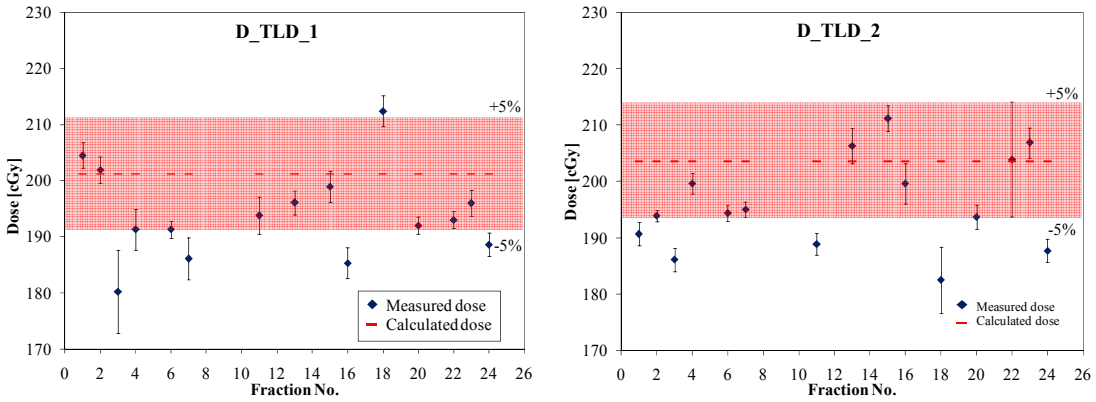

(b)

(c)

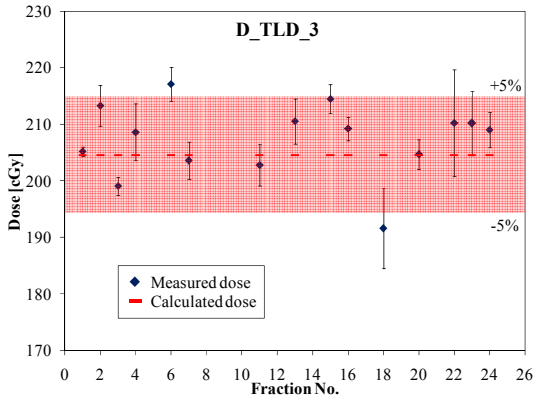

(d)

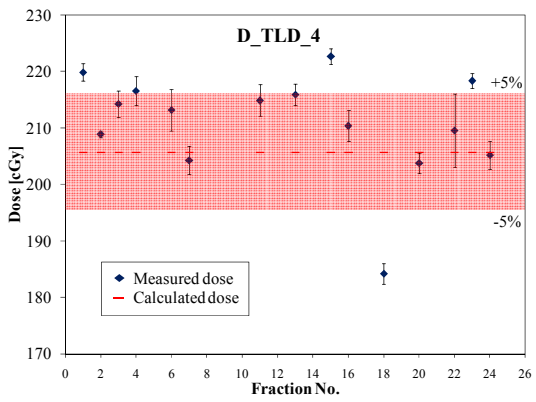

(e)

Figure 3.4. Patient D: (a) Picture of TLD placement and (b) through (e) Data comparing the calculated dose to TLD measured fractional daily dose at each TLD location. The pink region is the ±5% range about the calculated dose.

Table 3.6. Prescribed, calculated, mean TLD measured dose, and Dose difference between calculated and measured doses of patient E.

	Prescribed Doses		Calculated Doses	Measured Doses		Differences
TLD	fxs [#]	fx Dose [cGy]	[cGy]	N	$D \pm \sigma_D$ [cGy]	$\Delta \pm \sigma_\Delta$ [%]
1	25	200	200.8	15	199.5 ± 6.4	-0.6 ± 3.2
2	25	200	203.1	15	199.1 ± 7.7	-2.0 ± 3.8
3	25	200	201.7	15	196.5 ± 5.8	-2.6 ± 2.9
4	25	200	200.5	15	193.9 ± 9.3	-3.3 ± 4.7

patient A-E for the better comparison. A summary of the results will be shown and discussed later in this chapter. The 95% confidence interval (C.I.) for the regression line is given by equation (3).

$$Dose\ Difference\ [\%] = \frac{(Calculated\ Dose - Measured\ Dose)}{Calculated\ Dose} \times 100\% \qquad (2)$$

Each patient had 60 data points (15 fractions × 4 dose points/fraction) to correlate the dose difference to the air cavity volume and thickness. Best-fit linear regression to all the data points is shown on the plots along with the equation and R-squared value. Scales were kept the same for patient A-E for the better comparison. A summary of the results will be shown and discussed later in this chapter. The 95% confidence interval (C.I.) for the regression line is given by equation (3).

$$\hat{y}_i \pm t_{n-2} RMSE \sqrt{\frac{1}{n} + \frac{(x_i - \bar{x})^2}{\sum (x_i - \bar{x})^2}} \qquad (3)$$

where $\hat{y}_i$ is an equation-derived dose difference [%] value for each air volume and thickness data points measured, t_{n-2} is the t-distribution value obtained from excel stastiscal function (TINV), n is the number of sample, RMSE is root mean square error where $RMSE = \sqrt{\frac{\sum (y_i - \hat{y}_i)^2}{n-2}}$, and $\bar{x}$ is

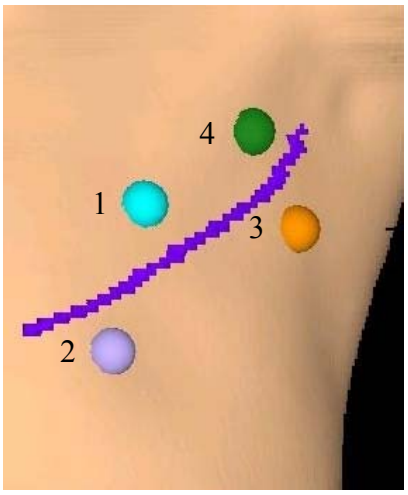

(a)

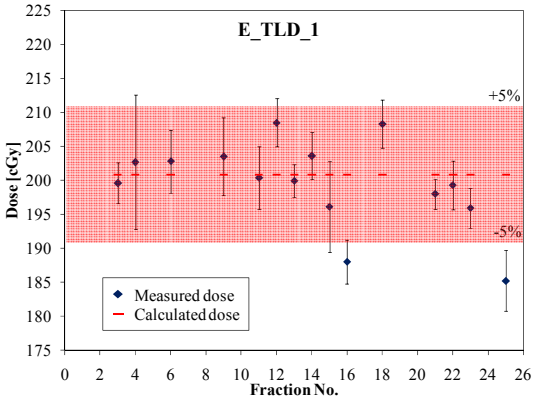

(b)

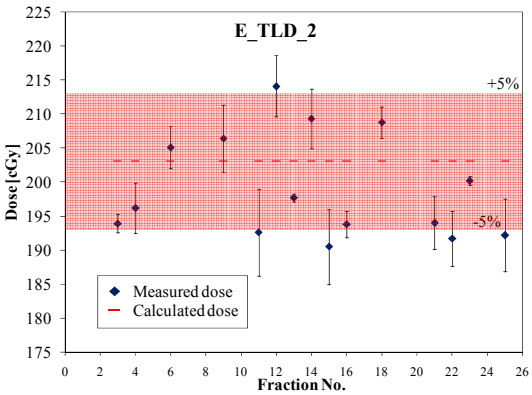

(c)

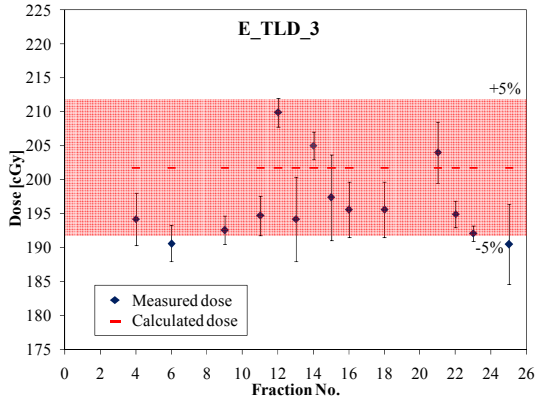

(d)

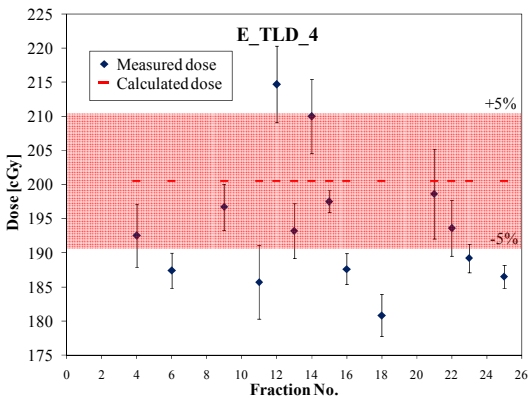

(e)

Figure 3.5. Patient E: (a) Picture of TLD placement and (b) through (e) Data comparing the calculated dose to TLD measured fractional daily dose at each TLD location. The pink region is the ±5% range about the calculated dose.

the average air volume or thickness, x, value. The C.I. is shown as red lines. The 95% prediction interval (P.I.) for the regression line is given by equation (4).

$$\hat{y}_i \pm t_{n-2} RMSE \sqrt{\frac{1}{n} + \frac{(x_i - \bar{x})^2}{\sum (x_i - \bar{x})^2} + 1} \quad (4)$$

The P.I. is shown as black dashed lines. Both C.I. and P.I. were calculated with Microsoft Excel spreadsheet.

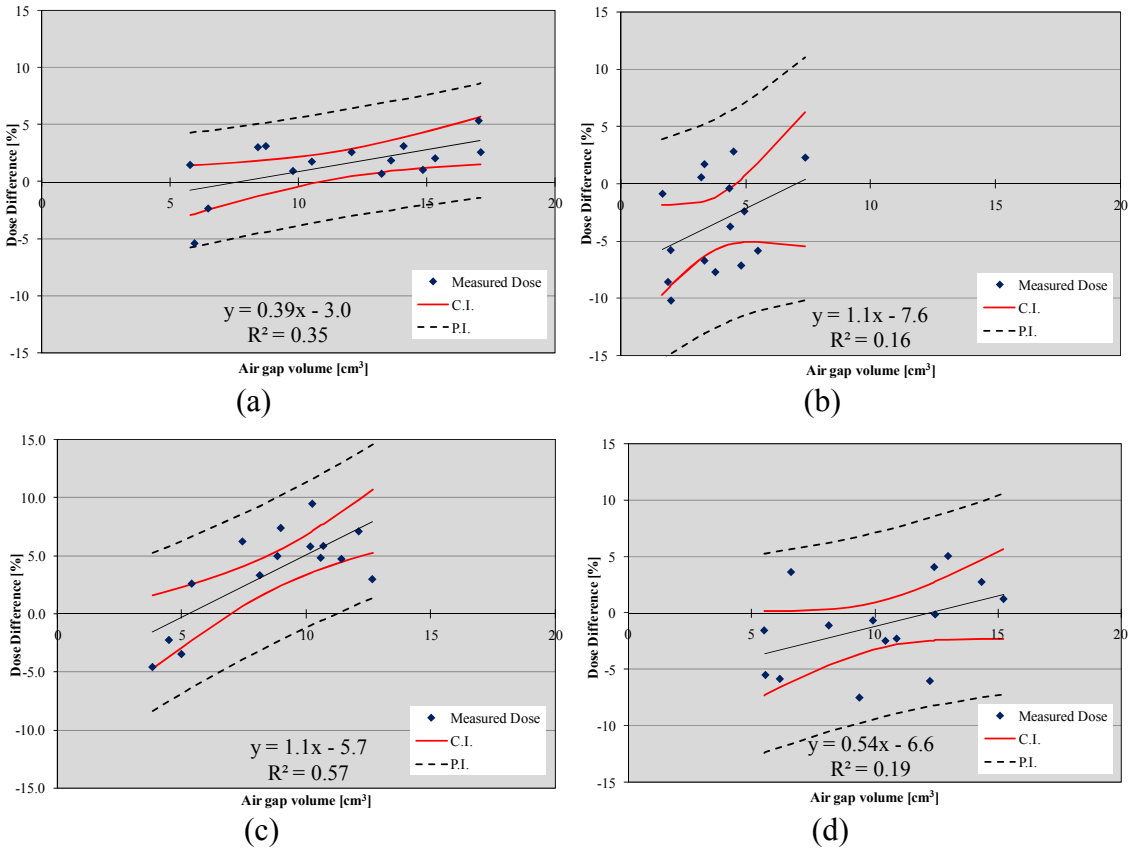

Figure 3.6. Patient A: Dose difference [%] of measured TLD dose and calculated dose versus air cavity volume for (a) TLD1, (b) TLD2, (c) TLD3, and (d) TLD 4.

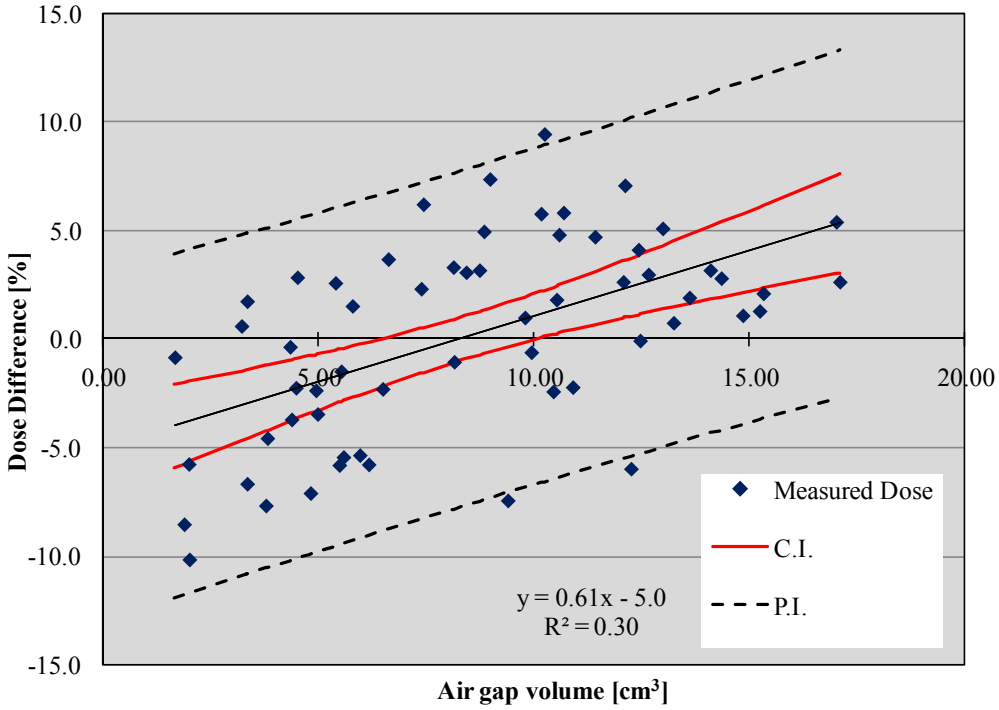

(a)

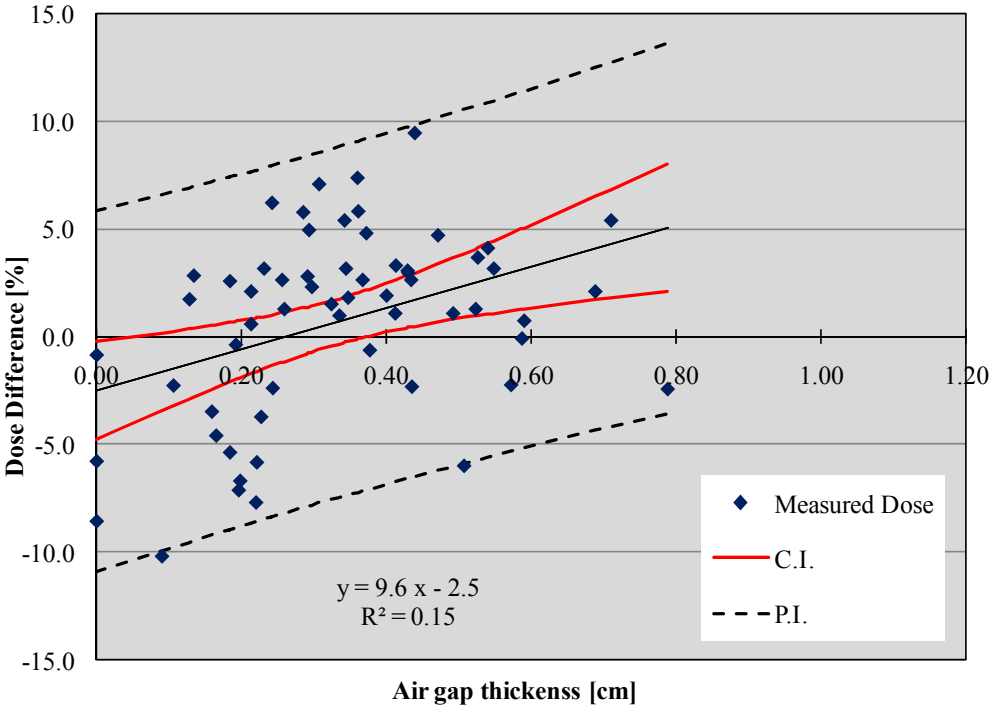

(b)

Figure 3.7. Patient A: (a) Dose difference [%] of measured TLD dose and calculated dose versus air cavity volume and (b) Dose difference [%] of measured TLD dose to the calculated dose versus air cavity thickness.

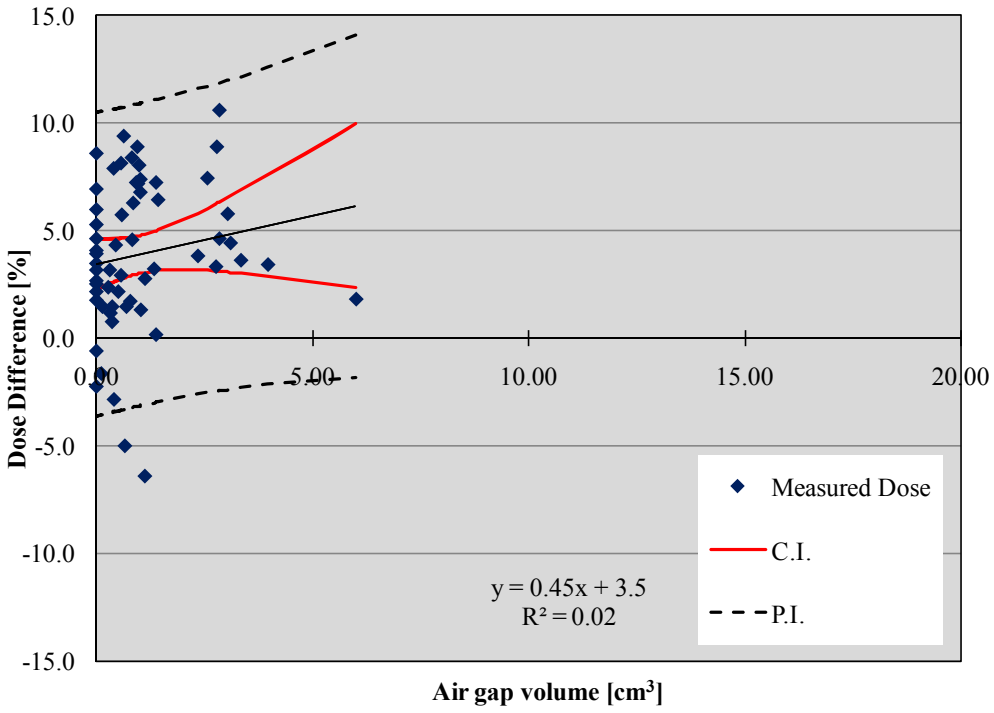

(a)

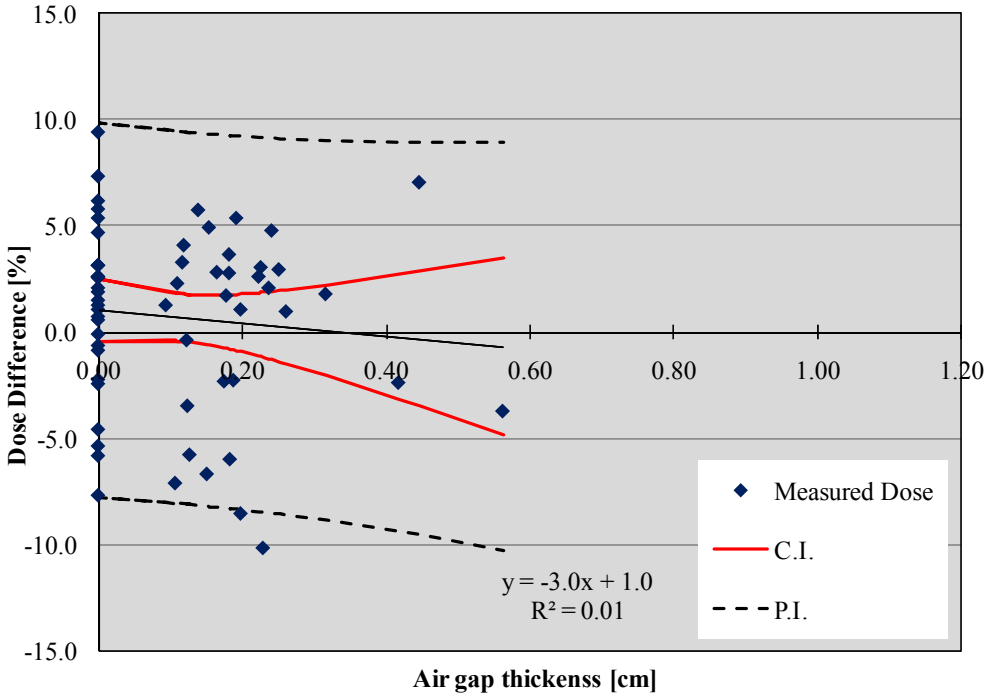

(b)

Figure 3.8. Patient B: (a) Dose difference [%] of measured TLD dose and calculated dose versus air cavity volume and (b) Dose difference [%] of measured TLD dose to the calculated dose versus air cavity thickness.

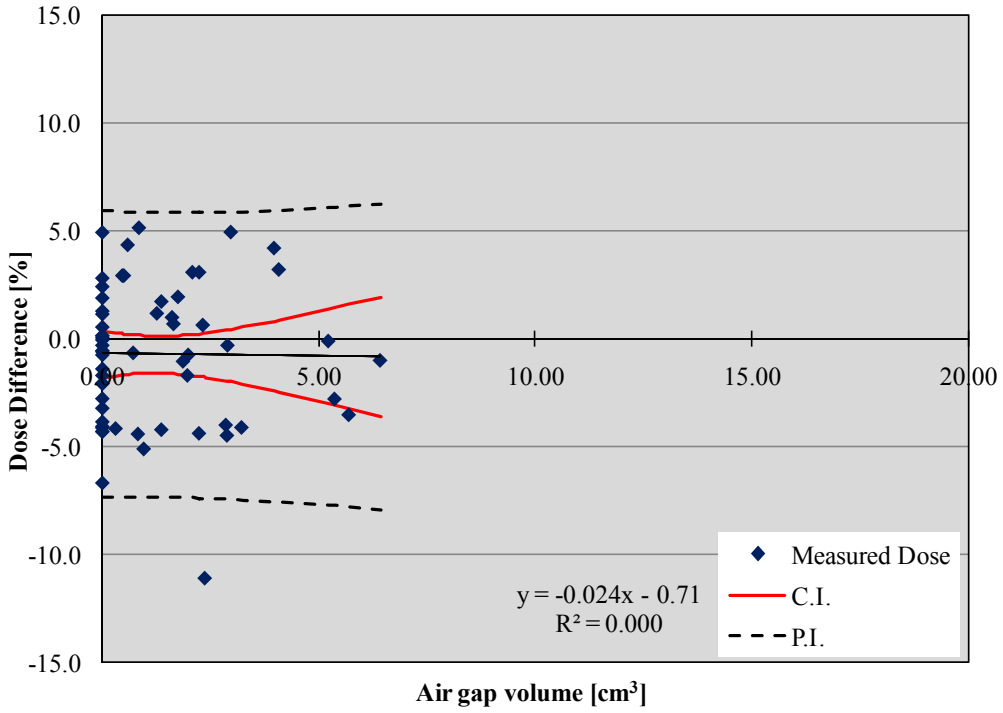

(a)

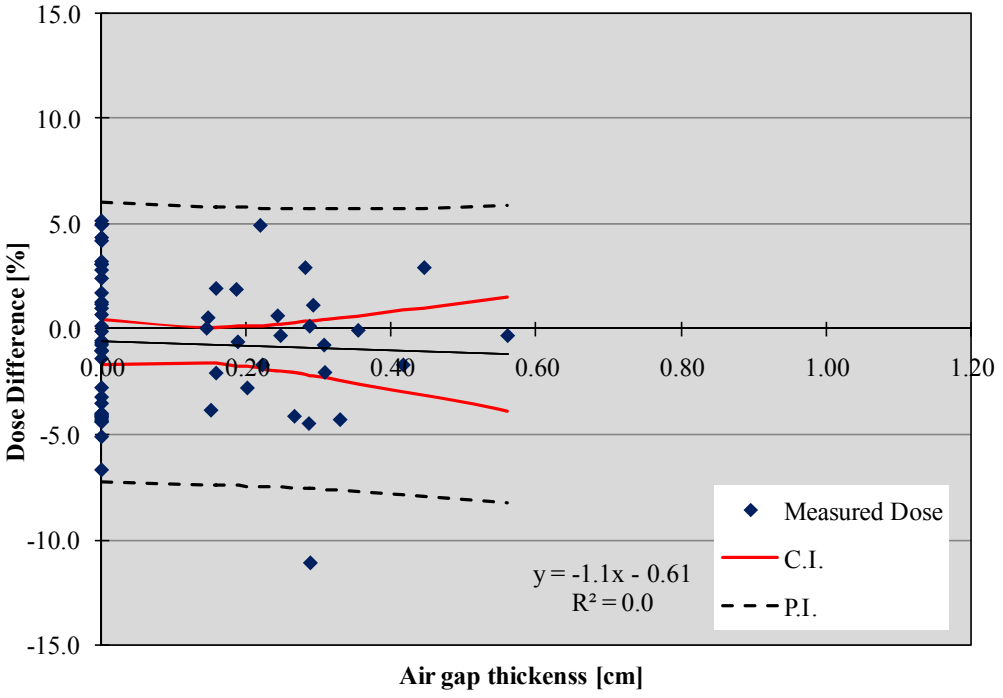

(b)

Figure 3.9. Patient C: (a) Dose difference [%] of measured TLD dose and calculated dose versus air cavity volume and (b) Dose difference [%] of measured TLD dose to the calculated dose versus air cavity thickness.

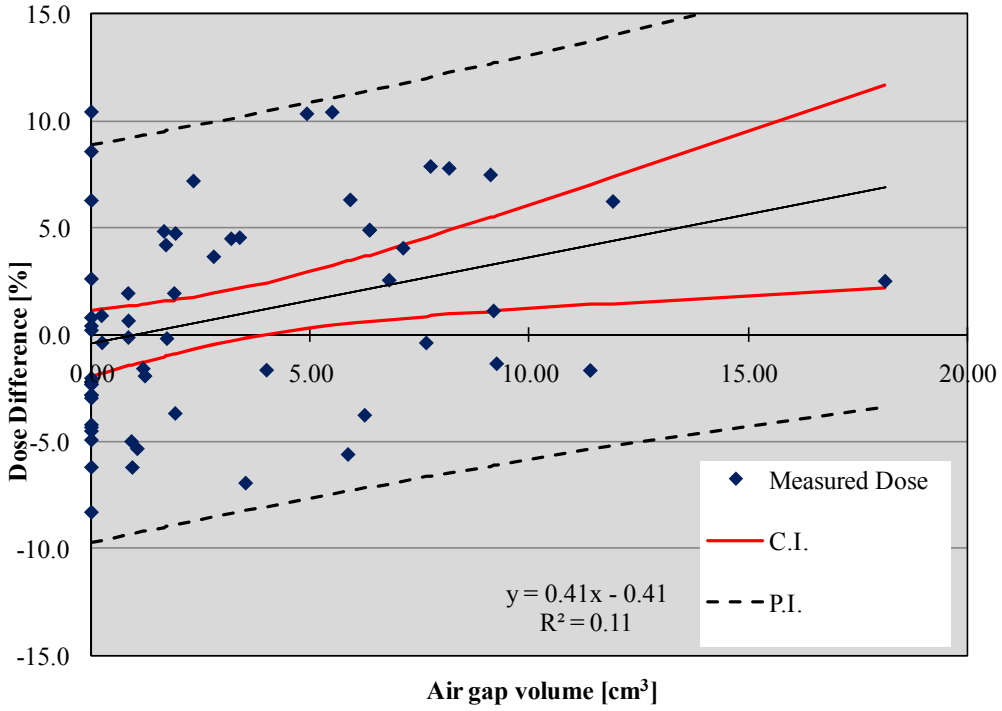

(a)

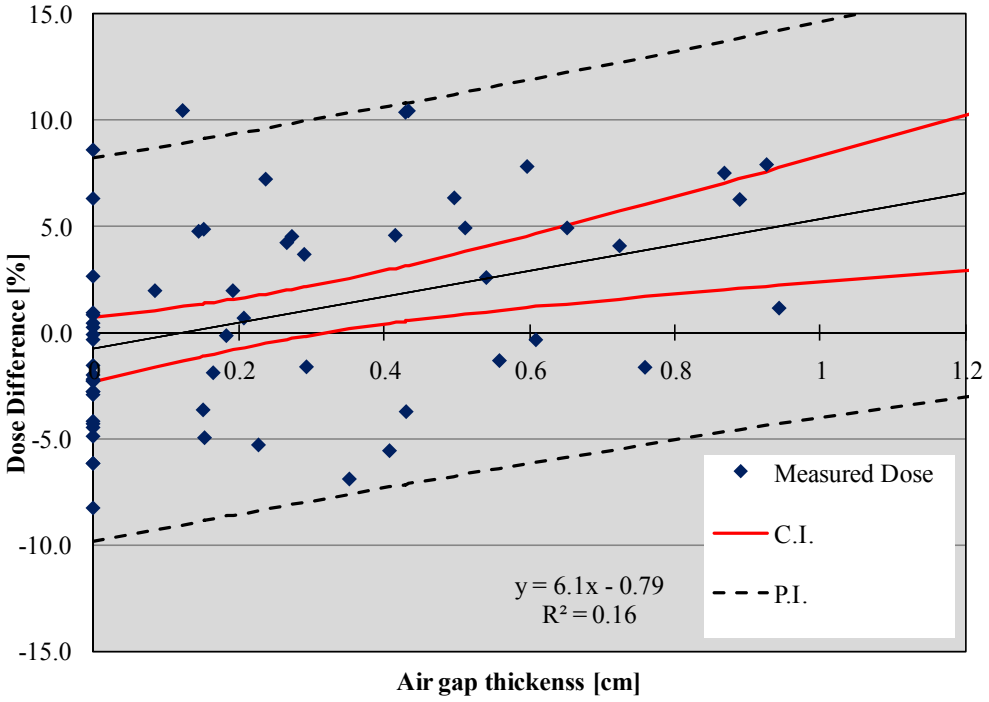

(b)

Figure 3.10. Patient D: (a) Dose difference [%] of measured TLD dose and calculated dose versus air cavity volume and (b) Dose difference [%] of measured TLD dose to the calculated dose versus air cavity thickness.

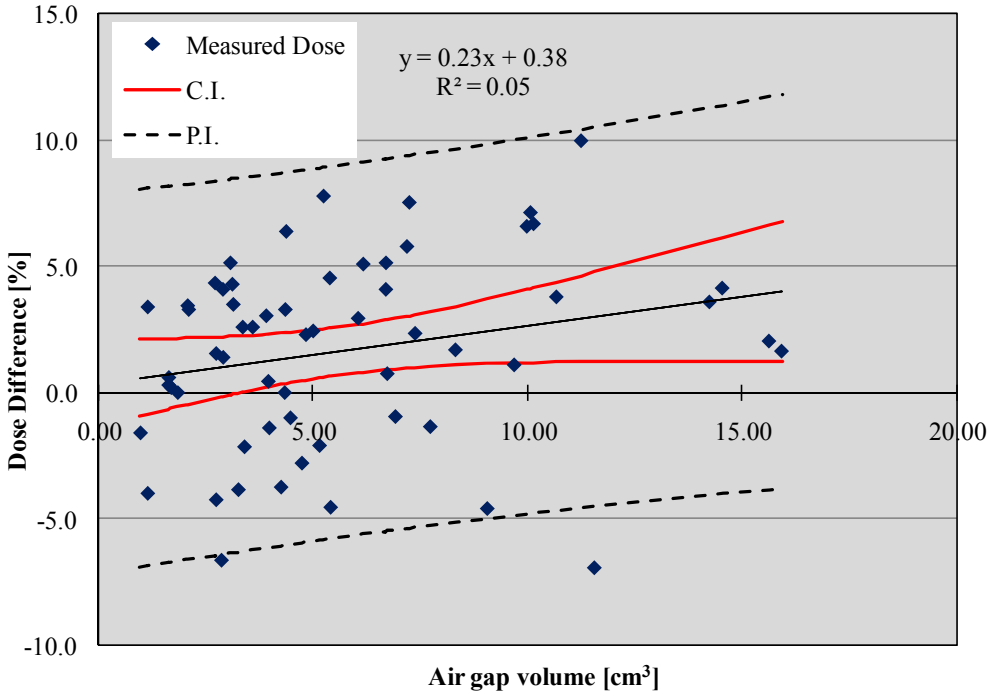

(a)

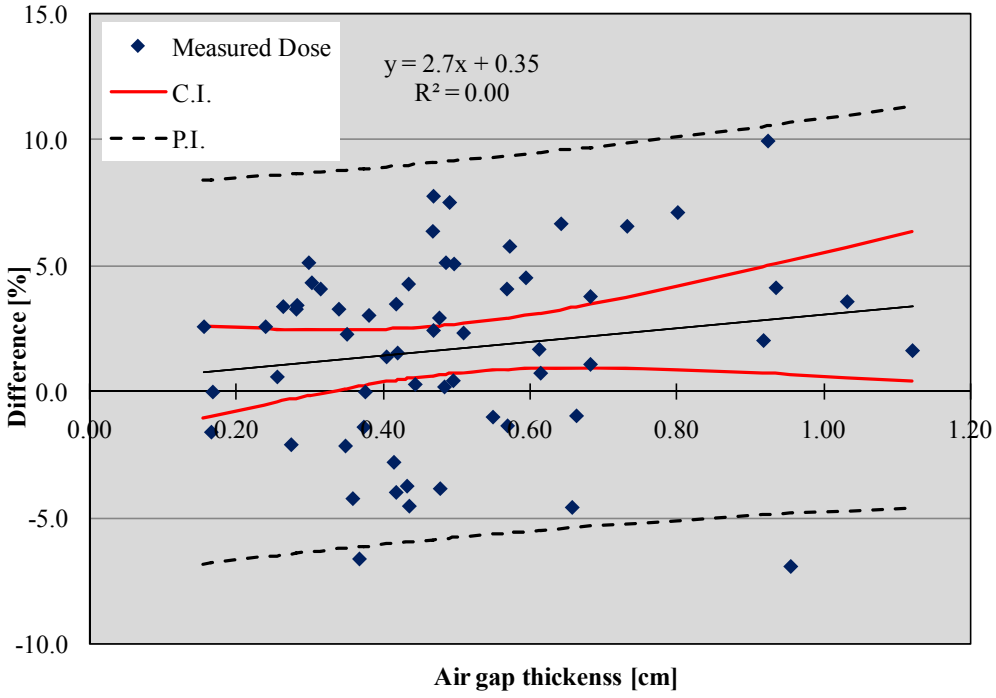

(b)

Figure 3.11. Patient E: (a) Dose difference [%] of measured TLD dose and calculated dose versus air cavity volume and (b) Dose difference [%] of measured TLD dose to the calculated dose versus air cavity thickness.

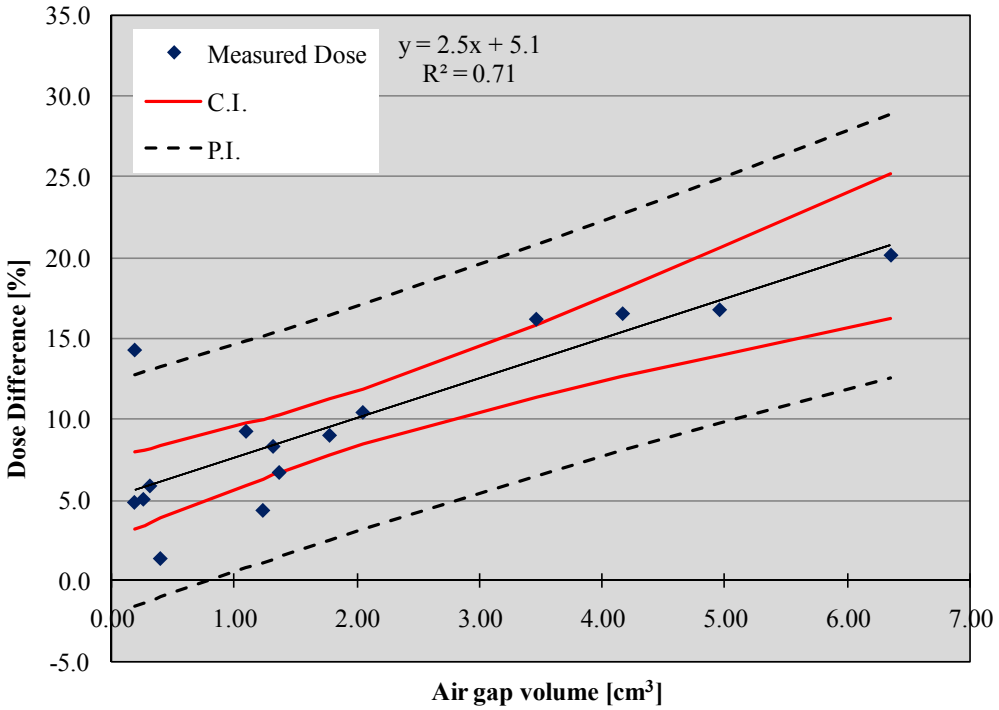

(a)

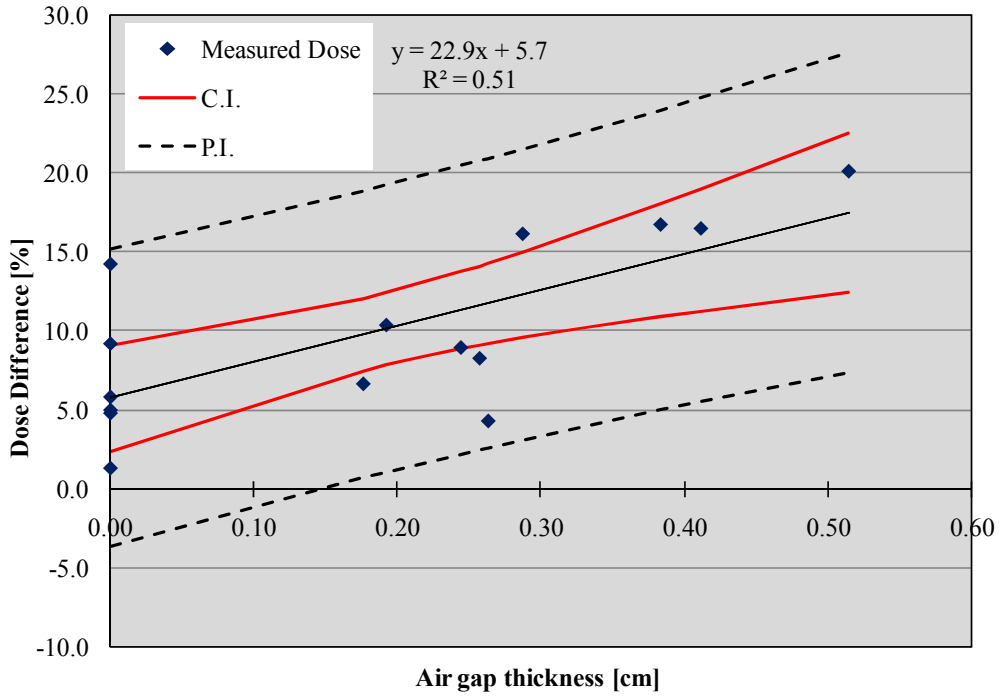

(b)

Figure 3.12. Patient F (cf. Fig 1.6c): (a) Dose difference [%] of measured TLD dose and calculated dose versus air cavity volume and (b) Dose difference [%] of measured TLD dose and calculated dose versus air cavity thickness for previous patient

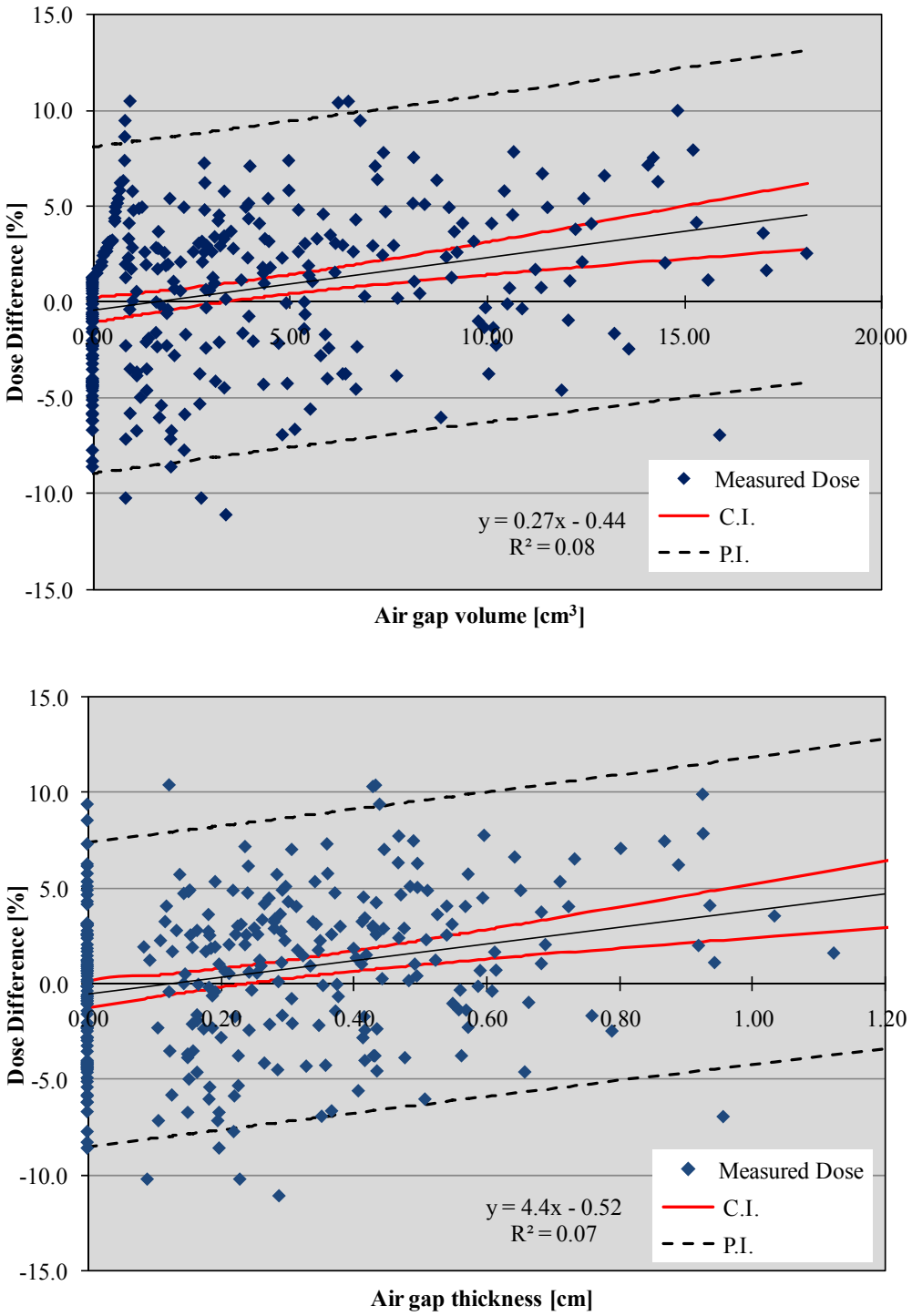

Figure 3.13. Patient A-E: (a) Dose difference [%] of measured TLD dose and calculated dose versus air cavity volume and (b) Dose difference [%] of measured TLD dose and calculated dose versus air cavity thickness for patient A-E combined.

III. Aim 3

A. TLD Measurements Tests

1. Accuracy and Precision of TLD Measurements Due to TLD System

Three sets of TLD were exposed to known doses (175, 200, and 225 cGy) and were treated as unknown sample doses. Calibration TLDs (3 per dose level) were exposed to 100, 150, 200, and 250 cGy to encompass the sample doses on the same day of sample TLDs delivery with the same linac. All TLDs were read the next day, and sample TLD readings were converted into dose using the dose calibration. Average measured TLD dose for each of the three "unknown" TLD sets was compared to expected dose, as shown in Table 3.7. Differences between measured and expected dose were calculated by using the equation (5).

$$\Delta(\%) = \frac{(\text{Avg Measured Dose} - \text{Expected Dose})}{\text{Expected Dose}} \times 100\% \qquad (5)$$

These results indicate that the TLD measurement system, used both for in-vivo patient dosimetry, as well as phantom measurements in the present study (discussed later in this chapter) was accurate to within 2%.

The precision of a single TLD reading is the standard deviation of the sample of three TLDs at each dose level. Expressed as a % ($100 \times \sigma/\bar{D}$), Table 3.6 shows values of 0.8, 1.1, and 0.3%, which average 0.7%, the estimated precision of a single TLD dose point.

Table 3.7. .Expected dose, average TLD measured dose, difference in percentage and their standard deviation is shown.

Expected Dose [cGy]	Avg TLD Dose $\bar{D} \pm \sigma_{\bar{D}}$ [cGy]	Difference $\Delta \pm \sigma_{\Delta}$ [%]
175	178.2 ± 1.4	1.8 ± 0.8
200	198.8 ± 2.2	-0.6 ± 1.1
225	227.9 ± 0.7	1.3 ± 0.3

2. Accuracy of TLD Dose Measurements in Anthropomorphic CW Phantom

The accuracy of patient measurements depends primary upon accuracy of TLD system, accuracy of TomoTherapy delivery, accuracy of the TomoTherapy treatment planning system, intrafraction patient motion, how well the bolus fits the patient, and possibly other patient dependent factors. As the present study is designed to evaluate dose inaccuracies due to patient effects, the present section looks at dose accuracy without such patient effects. This is done by comparing measured with calculated dose for an anthropomorphic CW phantom as shown in Figure 3.12.

Repeated CW surface dose measurements using the TLD system were taken on the anthromorphic CW phantom and compared with treatment planning (TP) calculated dose and also planned adaptive (PA) calculated dose. The phantom delivery was performed four times, one on one day and three on another. Each day, a single TLD was exposed at each location, and there were three readings per TLD, which produces a mean and standard deviation of the mean (as in section A).

After each treatment, the MVCT data was used to perform a Planned Adaptive dose calculation for comparison with the measured dose. This allowed the inaccuracy due to TomoTherapy delivery to be assessed. TP calculated dose, PA calculated dose, TLD measured dose, and percent difference between measured and calculated (both TP and PA). Doses at each TLD location (1-4) are shown in Tables 3.8a-d, respectively.

On day one, the PA calculated dose averaged 3.1% greater than the TP calculated dose. On days 2, 3, and 4, the PA calculated dose averaged 0.4% greater, 1.0% lesser, and 0.7% lesser than the TP calculated dose. Difference between measured and calculated dose was obtained from equation (2). TLD measured dose was consistently higher than both TP and PA calculated doses at TLD location 1 and generally lower at TLD location 2, 3, and 4. Calculated and PA dose

agreed well to within 3.1%, 0.4%, -1%, and -0.7% average at TLD location 1, 2, 3, and 4, respectively. Standard deviation for average difference in TLD measured and calculated dose did not exceed more than 2.4 % and 2.7% for average difference between TLD measured and planned adaptive dose. This result indicates that our TLD measurements are reliable as they can be reproduced to achieve within 2.4% uncertainty.

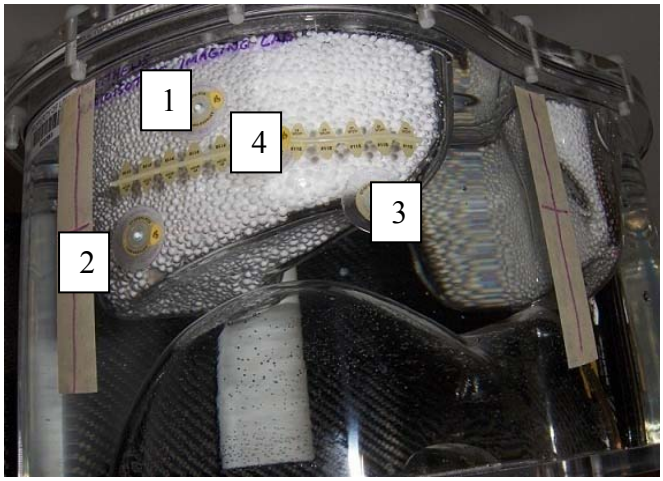

Figure 3.14. CW anthropomorphic phantom with 4 TLD locations.

3. Film Measurements

Film measured dose was compared with calculated dose to improve confidence in the accuracy of comparison between TLD dose measurements and the calculated dose, and the results are shown in Table 3.12. Average TLD measured dose was obtained from 4 repeated measurements shown in previous section and was compared with calculated dose. The film measurements were repeated twice to obtain uncertainty. Difference between average film measured dose and average TLD measured dose to the calculated dose were obtained from using equation (6).

$$\Delta_{Film/TLD}(\%) = \frac{(Avg\ Film/TLD\ Dose - Calculated\ Dose)}{Calculated\ Dose} \times 100 \qquad (6)$$

Table 3.8. (a)-(d) Calculated dose, plan adaptive dose, TLD measured dose, and difference between measured and calculated at each TLD location 1 through 4. (e) Summary of the results at 4 TLD locations. (TP = Treatment Planning, PA = Planned Adaptive)

TLD Location [#]	TP Calc. Dose [cGy]	PA Calc. Dose [cGy]	$\bar{D} \pm \sigma_{\bar{D}}$ [cGy]	Δ(PA-TP) [%]	Δ(TLD-TP) [%]	Δ(TL-PA) [%]
1	203.8	210.5	219.8 ± 0.2	3.3	7.8	4.4
1	203.8	210.0	217.8 ± 2.4	3.0	6.9	3.7
1	203.8	210.5	211.8 ± 1.5	3.0	3.9	0.6
1	203.8	210.5	216.7 ± 0.9	3.0	6.3	2.9
			Average	3.1	6.2	2.9

(a)

Table 3.9. (a)-(d) Calculated dose, plan adaptive dose, TLD measured dose, and difference between measured and calculated at each TLD location 1 through 4. (e) Summary of the results at 4 TLD locations. (TP = Treatment Planning, PA = Planned Adaptive)

TLD Location [#]	TP Calc. Dose [cGy]	PA Calc. Dose [cGy]	$\bar{D} \pm \sigma_{\bar{D}}$ [cGy]	Δ(PA-TP) [%]	Δ(TLD-TP) [%]	Δ(TL-PA) [%]
2	208.8	209.5	196.6 ± 3.5	0.3	-5.8	-6.2
2	208.8	210.0	206.3 ± 0.6	0.6	-1.2	-1.8
2	208.8	211.0	204.1 ± 2.2	1.1	-2.3	-3.3
2	208.8	207.5	208.0 ± 1.1	0.6	-0.4	-3.3
			Average	0.4	-2.4	-3.7

(b)

Table 3.10. (a)-(d) Calculated dose, plan adaptive dose, TLD measured dose, and difference between measured and calculated at each TLD location 1 through 4. (e) Summary of the results at 4 TLD locations. (TP = Treatment Planning, PA = Planned Adaptive)

TLD Location [#]	TP Calc. Dose [cGy]	PA Calc. Dose [cGy]	$\bar{D} \pm \sigma_{\bar{D}}$ [cGy]	Δ(PA-TP) [%]	Δ(TLD-TP) [%]	Δ(TL-PA) [%]
3	211.5	209.5	210.6 ± 2.3	-1.0	-0.4	0.5
3	211.5	209.5	204.7 ± 1.4	-1.0	-3.2	-2.3
3	211.5	210.5	201.2 ± 9.9	-0.5	-4.9	-4.4
3	211.5	208.5	199.4 ± 3.4	-1.4	-5.7	-4.4
			Average	-1.0	-3.6	-2.7

(c)

Table 3.11. (a)-(d) Calculated dose, plan adaptive dose, TLD measured dose, and difference between measured and calculated at each TLD location 1 through 4. (e) Summary of the results at 4 TLD locations. (TP = Treatment Planning, PA = Planned Adaptive)

TLD Location [#]	TP Calc. Dose [cGy]	PA Calc. Dose [cGy]	$\bar{D} \pm \sigma_{\bar{D}}$ [cGy]	Δ(PA-TP) [%]	Δ(TLD-TP) [%]	Δ(TL-PA) [%]
4	212.2	211.5	203.0 ± 3.7	-0.3	-4.3	-4.0
4	212.2	210.0	200.7 ± 2.6	-1.0	-5.4	-4.4
4	212.2	213.0	211.6 ± 0.6	0.4	-0.3	-0.7
4	212.2	208.5	204.0 ± 8.0	-1.7	-3.9	-2.2
			Average	-0.7	-3.5	-2.8

(d)

For TLD location 1, 2, 3, and 4, the agreement was excellent with a $\chi^2/\nu = 93.7$. Average dose difference between film measured dose and calculated dose was 0.7%, compared for -0.8 % for the TLDs but the average standard deviation of the film measurements at 4 different TLD location was 0.3 %, compared to 1.1 % for the TLDs, which indicates that the flim measurements were more reproducible than the TLD measurements. Calculated and film measured doses agreed to within 3.0 % of each other.

Table 3.12. Comparison between calculated dose, average film measured dose, dose difference between film and calculated and TLD and calculated. ($\chi^2\nu = 93.7$).

TLD location [#]	Calc. Dose [cGy]	$\bar{D} \pm \sigma_{\bar{D}}$ [cGy]	$\Delta_{Film} \pm \sigma_{\Delta}$ [%]	$\Delta_{TLD} \pm \sigma_{\Delta}$ [%]
1	203.8	210.3 ± 1.5	3.2 ± 0.7	6.2 ± 0.8
2	208.8	203.8 ± 0.1	-2.4 ± 0.0	-2.4 ± 1.2
3	211.5	210.2 ± 0.4	-0.6 ± 0.2	-3.6 ± 1.2
4	212.2	209.9 ± 0.9	-1.1 ± 0.4	-3.5 ± 1.1
		Avg	-0.2 ± 0.3	-0.8 ± 1.1

B. Impact of Intrafraction Motion

Result of dose differences between 3 CW treatment deliveries with 3 difference couch position at each TLD location are shown in Table 3.9. At TLD locations 1, 2, and 3 couch shift

(±1cm) had less than 3.2% difference in the measured dose when compared to measured dose with no couch shift. At TLD location 4, a +1cm couch shift measured 7% less dose than that with no shifts. Expect for that TLD reading, 1cm couch shift didn't have more than 3.2 % difference in dose when compared to no shift. The shift of 1cm applied to the couch is 6-7 times larger than the largest ant-post displacement (0.15cm) seen in the patient 4DCT data, thus the effect we would expect to see from our patient data should be much smaller and insignificant.

Table 3.13. Comparison of TLD measured dose between 3 different couch position at each TLD location. Δ(-1cm-0cm)/Δ(+1cm-0cm) indicate difference in dose between no couch shift delivery and -1 cm/+1 cm couch shift delivery.

TLD Location [#]	Calc Dose [cGy]	0 cm shift [cGy]	-1 cm shift [cGy]	Δ(-1cm-0cm) [%]	+1 cm shift [cGy]	Δ(+1cm-0cm) [%]
1	203.8	212.1	210.5	-0.8	205.6	-3.1
2	208.8	204.2	203.2	-0.5	197.6	-3.2
3	211.5	211.5	207.4	-1.9	213.9	1.1
4	212.2	212.2	207.8	-2.1	197.4	-7.0
			Avg	-1.3	**Avg**	-3.1

C. Impact of Foam Cavity Between Bolus and the Phantom Surface

The CW phantom was used to measure the surface dose with foam packing material, whose density was 15 times that of air, placed between the phantom and bolus. Plots of dose difference [%] of measured TLD dose and calculated dose versus foam gap volume and thickness are shown in Figure 3.13. Measurements were taken at 4 TLD locations and the thickness of foam gap was varied from 0 mm to 18 mm in increments of 3mm. A total of 28 data points were collected and used to correlate the dose difference to the volume (25 cm^2 × thickness) and thickness. Best-fit linear regression slope with its equation and R-square values are shown on the plot. The 95% C.I. and P.I. are also shown on the plot.

A summary of the results comparing best-fit values, 95% C.I., and goodness of fit for volume and thickness analysis of the patients and phantom is shown in Table 3.10. For the 5 patients data, dose difference (%) increased as air volume and thickness between the bolus and CW increased. The constants of proportionality varied significantly, ranging from 0.0 ± 0.3 to 0.6 ± 0.1 % cm^{-3} for the volume analysis and -3.0 ± 4.4 to 9.6 ± 3.0 % cm^{-1} for thickness analysis. For the previous patient F, the constants of proportionality were 2.5 ± 0.4 % cm^{-3} and 23 ± 6 % cm^{-1}, respectively, approximately a factor of 10 greater than values for patient A-E. Reasons for their differences are unknown. Contrastingly, for the CW phantom the constant of proportionality were 0.07 ± 0.04 % cm^{-3} and 1.8 ± 1.0 % cm^{-1}, not inconsistent with data for patient A-E. As expected with theory of electron disequilibrium, having air cavity above the target would lead to underdosing of the surface dose. Mean slope value obtained from patients A-E volume analysis data was 0.3 % cm^{-3} and 0.07 % cm^{-3} for the phantom. Mean slope value of thickness analysis for the patients was 2.9 % cm^{-1} and 1.8 % cm^{-1} for phantom data. However, R^2 values which indicates goodness of fit were extremely small for Patient A-E, averaging 0.1 for both volume and thickness analysis, and 0.12 for phantom data. Patient F showed the best R^2 value of 0.71 and 0.51 for volume and thickness, respectively, most likely due to the small number of data points collected compared to 5 patients and phantom study. Our extremely small R^2 values indicate that the amount of air cavity does not directly correlate to the fractional dose difference.

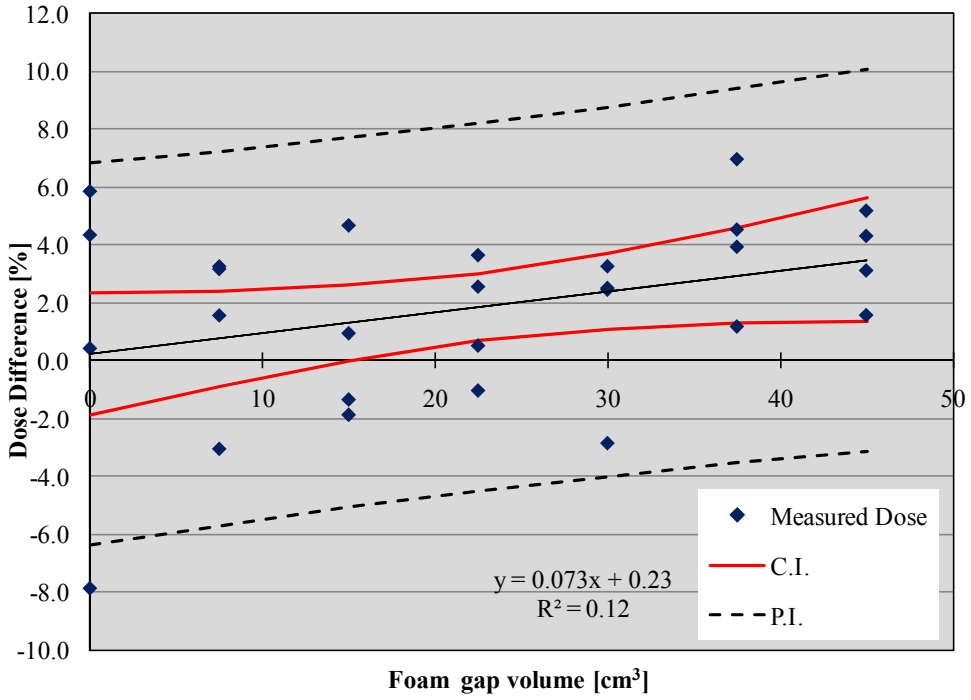

(a)

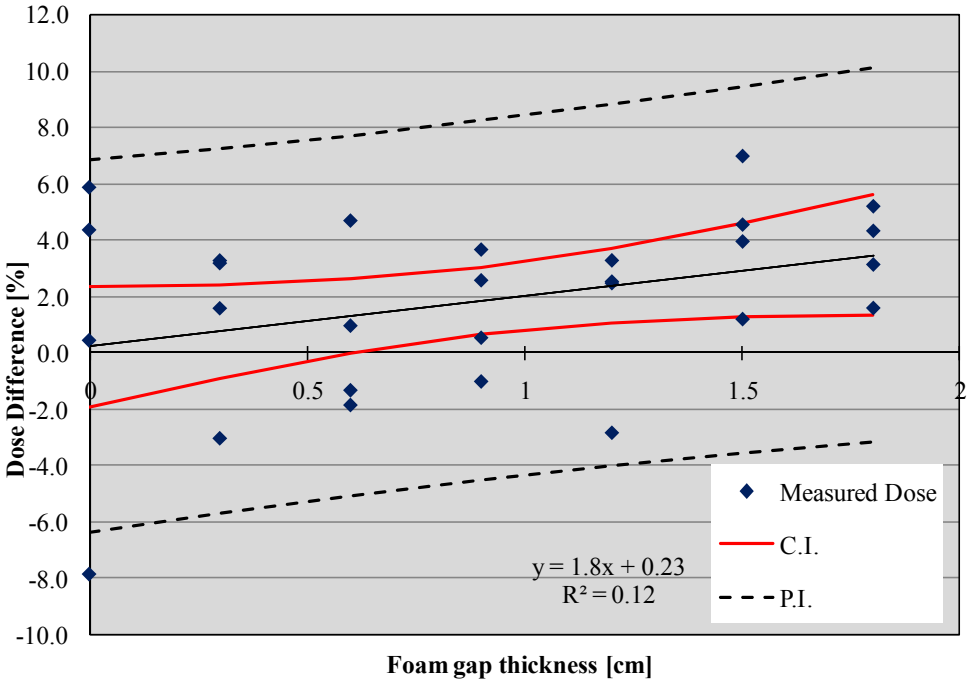

(b)

Figure 3.15. CW Phantom: (a) Dose difference [%] of measured TLD dose and calculated dose versus foam gap volume and (b) Dose difference [%] of measured TLD dose and calculated dose versus foam gap thickness. [Note: Plot (a) is plot (b) scaled by $(5.0\ cm)^2$.

Table 3.14. Summary of the results comparing best-fit values, 95% C.I., and goodness of fit for volume and thickness analysis of the patients and phantom

Volume

	Patient A	Patient B	Patient C	Patient D	Patient E	Patient F	CW Phantom
Best-fit values							
slope [% cm^{-3}]	0.61 ± 0.12	0.45 ± 0.38	-0.024 ± 0.26	0.41 ± 0.15	0.23 ± 0.13	2.5± 0.44	0.073 ± 0.038
Y-intercept when X=0.0	-5.0 ± 1.1	3.5 ± 0.6	-0.71 ± 0.53	-0.41 ± 0.76	0.38 ± 0.87	5.1 ± 1.2	0.23 ± 1.0
X-intercept when Y=0.0	8.3	-7.7	-29.8	1	-1.7	-2.1	-3.2
1/slope	1.6	2.2	-42.2	2.5	4.4	0.41	13.8
95% Confidence Intervals							
Slope [% cm^{-3}]	0.36 to 0.85	-0.30 to 1.20	-0.54 to 0.49	0.1 to 0.71	-0.027 to 0.48	1.5 to 3.4	-0.006 to 0.023
Y-intercept when X=0.0	-7.3 to -2.7	2.3 to 4.6	-1.8 to 0.5	-1.9 to 1.1	-1.4 to 2.1	2.6 to 7.6	-1.9 to 2.4
X-intercept when Y=0.0	6.4 to 10.0	-infinity to -2.1	-infinity to	-7.6 to 4.0	- infinity to 3.3	-4.7 to -0.8	-infinity to 15.1
Goodness of Fit							
r^2	0.3	0.02	0	0.11	0.05	0.71	0.12

Thickness

	Patient A	Patient B	Patient C	Patient D	Patient E	Patient F	CW Phantom
Best-fit values							
slope [% cm^{-1}]	9.6 ± 3.0	-3.0 ± 4.4	-1.1 ± 2.9	6.1 ± 1.8	2.7 ± 2.2	22.9 ± 6.2	1.8 ± 1.0
Y-intercept when X=0.0	-2.5 ± 1.1	1.0 ± 0.7	-0.61 ± 0.53	-0.79 ± 0.75	0.35 ± 1.2	5.7 ± 1.5	0.23 ± 1.0
X-intercept when Y=0.0	0.26	0.34	-0.56	0.13	-0.13	-0.25	-0.13
1/slope	0.1	-0.33	-0.91	0.16	0.37	0.04	0.55
95% Confidence Intervals							
Slope [% cm^{-1}]	3.5 to 15.6	-11.8 to 5.8	-6.8 to 4.6	2.5 to 9.8	-1.8 to 7.1	9.5 to 36.4	-0.16 to 3.8
Y-intercept when X=0.0	-4.8 to -0.22	-0.46 to 2.5	-1.7 to 0.4	-2.3 to 0.72	-2.1 to 2.8	2.4 to 9.1	-1.9 to 2.4
X-intercept when Y=0.0	0.052 to 0.37	-infinity to	-infinity to	-0.22 to 0.32	- infinity to 0.33	-0.88 to -0.07	-infinity to 0.60
Goodness of Fit							
r^2	0.15	0.01	0	0.16	0	0.51	0.12

Chapter 4
Conclusions

I. Response to Hypotheses

The hypothesis tested in this work was that the impact of intrafraction motion on TomoTherapy Post-Mastectomy Radiotherapy (PMRT) will be insignificant as (1) the largest intrafraction movement of the chest wall (CW) in the medial-lateral, anterior-posterior, and superior-inferior dimensions will not exceed 1 cm and (2) that 95% of in-vivo CW point doses on the patient surface will be within 5% of calculated dose and all doses within 10% of calculated dose.

The first hypothesis is true as the maximum ant-pos movements of our five patients were 0.15cm, 0.15cm, 0.11cm, 0.15cm, and 0.06cm respectively. The second hypothesis tested is not true due to the following: (1) for all the in-vivo CW point doses acquired on our five patients, 28% of the measured doses differed from the calculated dose by more than 5% and (2) 2% of all data differed from the calculated dose by more than 10%.

II. Clinical Impact and Clinical Recommendations

The results of this work indicate differences between TLD measured CW point dose and calculated dose, but overall, the fractional variation averaged out and none of the patient's total delivered dose differed from the calculated dose by more than 5%. Air cavities created between bolus and the patient's CW may lead to underdosing of the CW, however, larger number of patients data need to be studied before any numerical conclusion can be drawn to predict the amount of underdose. It is recommended that the air cavity be kept minimal by waiting until the bolus is completely dry before removing it from the patient at the time of fabrication. Proper positioning of the bolus to the CW for each treatment fraction should be verified by visual observation and evaluation of the positioning MVCT.

III. Future Work

A. Use of MVCT Data to Calculate the CW Dose

The present work used kVCT data acquired prior to treatment planning to calculate point dose on CW with TomoTherapy TPS. Using fractional MVCT image data to calculate the CW dose at each fraction and compare with the measured dose is of interest. Interfraction motion cause by anatomical change and/or positioning error could be a factor of discrepancy between measured and calculated dose.

B. Use of Planned Adaptive® Software to Calculate the CW Dose

Dose reconstruction, which combines the transmission data taken during the treatment with knowledge of the patient's anatomy and position to calculate the dose delivered to each region of the patient is possible with Planned Adaptive® software. (Ruchala *et al* 1999) Comparison between the planned adaptive calculated dose, using the daily MVCT data and the measured dose is yet to be studied.

C. Monte Carlo Calculation of TomoTherapy Delivery

TomoTheray TPS uses the convolution/superposition calculation algorithm. Full Monte Carlo calculation could be performed to verify the convolution/superposition calculated dose and compare the results of the Monte Carlo dose calculation algorithm with measured dose for both patients and phantom data.

References

American Cancer Society. *Breast Cancer Facts & Figures 2007-2008.* Atlanta: American Cancer Society Inc.

Ashenafi M, Boyd R, Lo K, Lee T, and Hogstrom K 2006 TomoTherapy for Post-Mastectomy Radiotherapy (PMRT): Comparison with Conventional Electron Beam Technique Louisianan State University Electronic Thesis & Dissertation Collection Located at http://etd.lsu.edu

Cheek D, Hogstrom K, Gibbons J, and Rosen I 2007: SU-FF-T-213: Evaluation of dose from tomotherapy irradiation of superficial PTVs *Med. Phys.* **34** 2450

Eifel P, Axelson JA, Costa J, Crowley J, Curran WJ Jr, Deshler A, Fulton S, Hendricks CB, Kemeny M, Kornblith AB, Louis TA, Markman M, Mayer R, and Roter D 2001 National Institute of Health Consensus Development Conference Statement: Adjuvant Therapy for breast cancer November 1-3 2000 *J.Natl. Cancer Inst.* **93** 979-989

Fitchard EE, Aldridge JS, Reckwerdt PJ, and Mackie TR 1998a Registration of synthetic tomograpic projection data sets using cross-correlation *Phys. Med. Biol.* **43** 1645-57

Fitchard EE, Aldridge JS, Reckwerdt PJ, Olivera GH, Mackie TR, and Iosevich A 1998b Six parameter patient registration directly from projection data *Nucl. Instrum. Methods Phys. Res.* A **421** 342-51

Han C, Chen Y, Lin A, Schultheiss T, and Wong J 2007 Dosimetric study and in-vivo dose verification for conformal avoidance treatment of anal adenocarcinoma using helical tomotherapy *Med. Dosimetry* **32** 33-37

Kanagaki B, Read PW, Molloy JA, Larner JM, and Sheng K 2007 A motion phantom study on helical tomotherapy: the dosimetric impacts of delivery technique and motion *Phys. Med. Biol.* **52** 243-55

Keall P, Mageras G, Balter J, Emery R, Forster K, Jiang S, Kapatoes J, Kubo H, Low D, Murphy M, Murray B, Ramsey C, van Herk M, Vedam S, Wong J, and Yorke E 2006 TG-76: The management of respiratory motion in radiation oncology

Lee T, Rosen I, Fields R, and Hogstrom K 2007 SU-FF-T-122: Comparison of helical tomotherapy to sMLC IMRT for treatment of parotid gland tumors *Med. Phys.* **34** 2429

Lu W, Fitchard EE, Olivera GH, You J, Ruchala KJ, Aldridge JS, and Mackie TR 1999 Image/patient registration from (partial) projection data by the Fourier phase matching method *Phys. Med. Biol.* **44** 2029-48

Mackie TR, Holmes T, Swerdloff S, Reckwert P, Deasy JO, Yang J, Paliwal B, and Kinsella T 1993 TomoTherapy: a new concept for the delivery of dynamic conformal radiotherapy *Med. Phys.* **20** 1709-19

Maor MH, Fields RS, Hogstrom KR, and Eys JV 1985 Improving the therapeutic ratio of craniospinal irradiation in medulloblastoma *Int. J. Radiat. Oncol. Biol. Phys.* **11**: 687-697

McNutt TR, Mackie TR, Reckwerdt PJ, and Paliwal BR 1996a Modeling dose distributions from portal dose using the convolution/superposition method *Med. Phys*. **23** 1381-92

McNutt TR, Mackie TR, Reckwerdt PJ, Papanikolaou N, and Paliwal BR 1996b Calculation of portal dose using the convolution/superposition method *Med. Phys*. **23** 527-35

Overgaard M, Hansen PS, Overgaard J, et al. 1997 Postoperative radiotherapy in high risk Premenopausal women with breast cancer who receive adjuvant chemotherapy: Danish Breast Cancer Cooperative Group 82b Trial. *N Engl J Med* **337** 949-955

Olivera GH, Shepard DM, Ruchala K, Aldridge JS, Kapatoes JM, Fitchard EE, Reckwerdt PJ, Fang G, Balog J, (Madison, WI: Medical Physics Publishing) pp 521-87

Orton N, Jaradat H, Welsh J, and Tomé W 2005 Total scalp irradiation using helical tomotherapy *Med. Dosimetry* **30** 162-168

Overgaard M, Jensen MB, Overgaard J, et al. 1999 Postoperative radiotherapy in high risk post menopausal breast-cancer patients given adjuvant tamoxifen: Danish Breast Cancer Cooperative Group DBCG 82c randomized trial. Lancet **353** 1641-1648

Pierce L, Butler J, Martel M, Normolle D, Koelling T, Marsh R, Lichter A, and Fraass B 2002 Postmastectomy radiotherapy of the chest wall: dosimetric comparison of common Techniques *Int. J. Radiation Oncology Biol. Phys.* 52 1220-1230

Rietzel E, Pan T, Chen G 2005 Four-dimensional computed tomography: Image formation and Clinical protocol *Med. Phys*. **32** 874-889

Ruchala K, Olivera G, Schloesser E, and Mackie T 1999 Megavolatage CT on a tomotherapy system *Phys. Med. Biol.* **44** 2597-2621

Strom EA, McNeese MD, Fletcher GH, et al. Results of mastectomy and postoperative irradiation in the management of locoregionally advanced carcinoma of the breast. *Int J Radiat Oncol Biol Phys* 1991;21:319-323.

Tomblyn M, Hui S, and Dusenbery K 2007 SU-FF-T-130: Conformal avoidance and helical therapy utility in craniospinal radiation *Med. Phys.* **34** 2431

Tung S, Shiu A, Starkschall G et al. 1993 Dosimetric evaluation of total scalp irradiation using a lateral electron-photon technique. *Int. J. Radiat. Oncol. Biol. Phys.* **27**: 153-60

Yang J, Mackie T, Reckwerdt P, Deasy J, and Thomadsen B 1996 An investigation of tomotherapy beam delivery *Med. Phys.* **24** 425-436

Yu X, Jaffray D, and Wong J 1998 The effects of intra-fraction organ motion on the delivery of Dynamic intensity modulation *Phys. Med. Biol.* **43** 91-104

Appendix: List of Acronyms

4DCT: 4 Dimensional CT

CT: Computed Tomography

CW: Chest Wall

DTA: Distance To Agreement

IGRT: Image-Guided Radiation Therapy

IMNs: Internal Mammary Nodes

IMRT: Intensity Modulated Radiation Therapy

kVCT: kilo-Voltage Computed Tomography

LINAC: Linear Accelerator

MBPCC: Mary Bird Perkins Cancer Center

MLC: Multi Leave Collimator

MR: Magnetic Resonance

MSCT: Multi-Slice CT

MVCT: Mega-Voltage Computed Tomography

PMRT: Post Mastectomy Radiotherapy

PTV: Planning Target Volume

PWTF: Partially Wide Tangent Field

RHS: Reverse Hockey Stick

RPM: Respiratory Gating System

RT: Radiation Therapy

sMLC: segmented Multi Leave Collimator

TLD: Thermoluminescent Dosimeter

TPS: Treatment Planning System

Vita

Shima Ito was born in Tokyo, Japan, in 1981, the only daughter of Akira Ito and Hiroko Koyama-Ito. At the age of 11, she travelled to North America for the first time to accompany her father's attendance to an AAPM annual meeting in Calgary, Canada. She attended Cypress Spring High School in Katy, Texas, from 1996 to 1997 as an exchange student and returned to Japan to complete her work at Tokyo Jogakkan High School. In 2001, she entered Bates College in Lewiston, Maine, to pursue a degree in physics. During her 4 years as an undergraduate, she spent a semester in London, United Kingdom, and a semester at Tulane University in New Orleans, Louisiana. In August 2005, she began her master's work at Louisiana State University. She is now a candidate for the degree of Master of Science in Medical Physics.